

NASA/TM-2016-219193



A Coupled Probabilistic Wake Vortex and Aircraft Response Prediction Model

*Thijs Gloudemans, Sander Van Lochem, and Eelco Ras
Delft University of Technology, Delft, Netherlands*

*Joel Malissa
University of Pennsylvania, Philadelphia, Pennsylvania*

*Nashat N. Ahmad and Timothy A. Lewis
Langley Research Center, Hampton, Virginia*

NASA STI Program . . . in Profile

Since its founding, NASA has been dedicated to the advancement of aeronautics and space science. The NASA scientific and technical information (STI) program plays a key part in helping NASA maintain this important role.

The NASA STI program operates under the auspices of the Agency Chief Information Officer. It collects, organizes, provides for archiving, and disseminates NASA's STI. The NASA STI program provides access to the NTRS Registered and its public interface, the NASA Technical Reports Server, thus providing one of the largest collections of aeronautical and space science STI in the world. Results are published in both non-NASA channels and by NASA in the NASA STI Report Series, which includes the following report types:

- **TECHNICAL PUBLICATION.** Reports of completed research or a major significant phase of research that present the results of NASA Programs and include extensive data or theoretical analysis. Includes compilations of significant scientific and technical data and information deemed to be of continuing reference value. NASA counter-part of peer-reviewed formal professional papers but has less stringent limitations on manuscript length and extent of graphic presentations.
- **TECHNICAL MEMORANDUM.** Scientific and technical findings that are preliminary or of specialized interest, e.g., quick release reports, working papers, and bibliographies that contain minimal annotation. Does not contain extensive analysis.
- **CONTRACTOR REPORT.** Scientific and technical findings by NASA-sponsored contractors and grantees.

- **CONFERENCE PUBLICATION.** Collected papers from scientific and technical conferences, symposia, seminars, or other meetings sponsored or co-sponsored by NASA.
- **SPECIAL PUBLICATION.** Scientific, technical, or historical information from NASA programs, projects, and missions, often concerned with subjects having substantial public interest.
- **TECHNICAL TRANSLATION.** English-language translations of foreign scientific and technical material pertinent to NASA's mission.

Specialized services also include organizing and publishing research results, distributing specialized research announcements and feeds, providing information desk and personal search support, and enabling data exchange services.

For more information about the NASA STI program, see the following:

- Access the NASA STI program home page at <http://www.sti.nasa.gov>
- E-mail your question to help@sti.nasa.gov
- Phone the NASA STI Information Desk at 757-864-9658
- Write to:
NASA STI Information Desk
Mail Stop 148
NASA Langley Research Center
Hampton, VA 23681-2199

NASA/TM-2016-219193



A Coupled Probabilistic Wake Vortex and Aircraft Response Prediction Model

*Thijs Gloudemans, Sander Van Lochem, and Eelco Ras
Delft University of Technology, Delft, Netherlands*

*Joel Malissa
University of Pennsylvania, Philadelphia, Pennsylvania*

*Nashat N. Ahmad and Timothy A. Lewis
Langley Research Center, Hampton, Virginia*

National Aeronautics and
Space Administration

Langley Research Center
Hampton, Virginia 23681-2199

May 2016

The use of trademarks or names of manufacturers in this report is for accurate reporting and does not constitute an official endorsement, either expressed or implied, of such products or manufacturers by the National Aeronautics and Space Administration.

Available from:

NASA STI Program / Mail Stop 148
NASA Langley Research Center
Hampton, VA 23681-2199
Fax: 757-864-6500

Contents

Contents	iii
List of Acronyms, Abbreviations, and Symbols.....	v
1. Introduction.....	1
Aircraft VOrtex Spacing System (AVOSS).....	1
Wake Vortex Scenarios Simulation (WakeScene) Package.....	2
Wake4D.....	2
Wirbelschleppen- Vorhersage- und Beobachtungssystem (WSVBS).....	3
Wake Turbulence Re-Categorization Program	4
A Coupled Probabilistic Wake and Aircraft Response Prediction Model.....	6
2. Probabilistic Wake Vortex Modeling	7
Fast-Time Wake Vortex Decay and Transport Models.....	7
AVOSS (Aircraft Vortex Spacing System) Prediction Algorithm (APA).....	8
TASS (Terminal Area Simulation System) Driven Algorithms for Wake Prediction (TDP).....	8
Wake Vortex Field Experiments.....	8
Memphis 1995 Wake Vortex Field Experiment	8
Denver 2006 Wake Vortex Field Experiment	9
Data Processed for Fast-Time Wake Models.....	9
Aircraft Data.....	9
Crosswinds	9
Eddy Dissipation Rate	10
Stratification	10
Monte Carlo Simulation Methodology	11
Generation of Initial Conditions.....	11
Simulation Results.....	16
3. Aircraft Response Modeling	18
Vortex Encounter Metrics.....	18
Vortex Circulation Strength.....	18
Rolling Moment Coefficient	18
Roll Angle	18
Roll Control Ratio.....	19

Bowles-Tatnall Method	19
Evaluation using Wind Tunnel Data	21
Correction to the Bowles-Tatnall Method	22
4. Wake Encounter Analysis	27
5. Summary	31
Acknowledgment.....	33
Appendix A: Derivation of Rolling Moment Coefficient.....	33
Appendix B: Calculation of C_{lv} at Time t	37
Appendix C: Sensitivity to Vortex Model	37
Idealized Vortex Models	37
Lamb-Oseen Model.....	37
Burnham-Hallock Model.....	37
Proctor Model.....	37
Rankine Model	38
Winckelmans Model	38
Jacquin Model.....	38
Sensitivity Analysis	39
Appendix D: Maximum Vortex-Induced Roll Angle.....	41
References.....	41

List of Acronyms, Abbreviations, and Symbols

ADS-B	Automatic Dependent Surveillance – Broadcast
AFR	Autonomous Flight Rules
AGL	Above Ground Level
APA	AVOSS Prediction Algorithm
ASOS	Automated Surface Observations System
ATC	Air Traffic Control
ATM	Air Traffic Management
AVOSS	Aircraft VOrtex Spacing System
AWIATOR	Aircraft Wing Advanced Technology Operations
CREDOS	Crosswind-Reduced Separations for Departure Operations
D2P	Deterministic Two Phase model
DEN	Denver International Airport
DFW	Dallas/Fort Worth International Airport
DEN06	Denver 2006 Wake Vortex Field Experiment (NASA)
DLR	Deutsches Zentrum für Luft- und Raumfahrt
DVM	Deterministic wake Vortex Model
EDR	Eddy Dissipation Rate (m^2/s^3)
EGPWS	Enhanced Ground Proximity Warning System
FAA	Federal Aviation Administration
FACET	Future ATM Concepts Evaluation Tool
FAR-Wake	Fundamental Research on Aircraft Wake Phenomena
ICAO	International Civil Aviation Organization
IGE	In-Ground Effect
IFR	Instrument Flight Rules
IM	Interval Management
IMC	Instrument Meteorological Conditions
LES	Large Eddy Simulation
Lidar	LIght Detection And Ranging
mae	Mean Absolute Error
MEM	Memphis International Airport
MEM95	Memphis 1995 Wake Vortex Field Experiment
MRS	Minimum Radar Separation
MTOW	Maximum Takeoff Weight
NAS	National Airspace System
NASA	National Aeronautics and Space Administration
NGE	Near-Ground Effect
NOWVIV	NOwcasting Wake Vortex Impact Variables
NTSB	National Transportation Safety Board
NWS	National Weather Service
OGE	Out-of-Ground Effect
P2P	Probabilistic Two-Phase model

pdf	Probability Density Function
PVM	Probabilistic wake Vortex Model
RASS	Radio Acoustic Sounding System
RCR	Roll Control Ratio
RECAT	FAA's Wake Turbulence Re-categorization Program
RMC	Roll Moment Coefficient severity metric
rmse	root mean square error
SAPA	Simplified Aircraft-Based Paired Approach
SHAPE	Simplified Hazard Area Prediction
SODAR	SOmic Detection And Ranging
SWIM	System-Wide Information Management
TASS	Terminal Area Simulation System
TDP	TASS Driven Algorithms for Wake Prediction
UCL	Université catholique Louvain
VESA	Vortex Encounter Severity Assessment
VMC	Visual Meteorological Conditions
WakeScene	Wake Vortex Scenarios Simulation
WSVBS	Wirbelschleppen- Vorhersage- und Beobachtungssystem
q	Vortex-induced angle of attack (rad)
b_0	Initial vortex pair separation (m)
b	Wingspan (m)
ε	Eddy Dissipation Rate (m^2/s^3)
ρ	Air density (kg/m^3)
θ	Potential Temperature/Theta (K)
V_0	Initial vortex pair descent velocity (m/s)
y_0	Initial position of the vortex pair with respect to the runway centerline (m)
z_0	Initial vortex height AGL (m)
$\delta_{a,\max}$	Maximum aileron deflection (rad)
Γ	Vortex circulation (m^2/s)
Γ_0	Initial vortex circulation (m^2/s)
Γ^*	Vortex circulation strength normalized by initial vortex strength, Γ_0
λ_F	Following aircraft wing taper ratio (-)
ϕ	Bank angle of the following aircraft (rad)
ϕ_∞	Bank angle asymptotically approached during vortex encounter without control input
ϕ_{\max}	Vortex-induced maximum bank angle (rad)
$(AR)_G$	Aspect ratio of the generating aircraft wing (-)
b_F	Following aircraft wing span (m)
b_G	Generating aircraft wing span (m)
c_F	Following aircraft wing chord (m)
$C_{L\alpha F}$	Three-dimensional lift-curve slope of following aircraft (rad^{-1})

$C_{l_{\delta\alpha}}$	Aileron effectiveness coefficient (-)
C_{l_c}	Control input roll moment coefficient (-)
C_{l_G}	Lift coefficient of the generating aircraft (-)
$C_{l_{\bar{p}}}$	Roll damping coefficient (rad^{-1})
C_{l_v}	Vortex-induced rolling moment coefficient (-)
g	Earth's gravitational acceleration (m/s^2)
I_{xx}	Roll moment of inertia ($\text{kg}\cdot\text{m}^2$)
l_v	Rolling moment (m-kg)
N	Dimensional Brunt-Väisälä frequency
N^*	Non-dimensional Brunt-Väisälä frequency
\bar{q}	Freestream dynamic pressure (kg/m^2)
r	Radial distance from vortex center (m)
r_c	Vortex-core radius (m)
r_i	Internal vortex core radius (m)
r_o	External vortex core radius (m)
s	Half vortex pair separation (m) = $b_0/2$
S_F	Following aircraft wings planform area (m^2)
t	Vortex age
T	Non-dimensional time (-)
T_c	Control input activation time (s)
T_m	Time at which the bank angle reaches a maximum (s)
T_v	Vortex impulse deactivation time (s)
V_F	Velocity of the following aircraft (m/s)
V_G	Generating aircraft velocity (m/s)
V_θ	Vortex tangential velocity (m/s)
w_G	Generating aircraft weight (kg)
w_T	Tangential vortex velocity component (m/s)
w_Y	Lateral vortex velocity component (m/s)
w_Z	Vertical vortex velocity component (m/s)
w_{b_y}	Total lateral vortex-induced velocity component (m/s)
w_{b_z}	Total vertical vortex-induced velocity component (m/s)
Y	Inertial lateral coordinate (m)
Y_F	Lateral location of the following aircraft (m)
Y^*	Lateral position of the vortex non-dimensionalized by b_0 (-)
Z	Inertial vertical coordinate (m)
Z_F	Vertical location of the following aircraft (m)
Z^*	height of the vortex non-dimensionalized by b_0 (-)

1. Introduction

Wake vortex spacing standards along with weather and runway occupancy time, restrict terminal area throughput and impose major constraints on the overall capacity and efficiency of the National Airspace System (NAS). For more than two decades, the National Aeronautics and Space Administration (NASA) has been conducting research on characterizing wake vortex behavior in order to develop fast-time wake transport and decay prediction models. It is expected that the models can be used in the systems level design of advanced air traffic management (ATM) concepts that safely increase the capacity of the NAS. It is also envisioned that at a later stage of maturity, these models could potentially be used operationally, in ground-based spacing and scheduling systems as well as on the flight deck.

This section gives a brief overview of past efforts in the United States and in Europe, on developing capacity enhancing procedures and tools based on wake modeling and/or wake vortex measurements. The need for a probabilistic wake model that is coupled with an aircraft response model for air traffic management applications is also discussed.

Aircraft Vortex Spacing System (AVOSS)

NASA's Aircraft Vortex Spacing System (AVOSS) was designed to maximize runway acceptance rates by dynamically adapting the spacing criteria to ambient meteorological conditions (Hinton 1995; Perry et al. 1997; O'Connor and Rutishauser 2001). AVOSS was designed for single runway approaches, but can be extended to other operational scenarios in the terminal area. The concept made use of both wake prediction models and field wake sensors to validate the model predictions. The deployed sensors included two instrumented towers; Radio Acoustic Sounding System (RASS) for temperature measurements; and, SODAR and Doppler radar for wind measurements. The measurements were used to generate vertical profiles of background atmospheric turbulence, winds, and temperature at thirty minutes intervals. These profiles served as the short-term weather forecast and were used to initialize the wake vortex decay and transport prediction models (O'Connor and Rutishauser 2001). Wake vortex measurements were obtained from continuous wave lidar (Figure 1.1).

To determine the probability of a wake vortex encounter, AVOSS considered the strength of vortices present within the boundaries of the approach and departure corridors used by the aircraft. To create the corridors a 3σ buffer was applied to the observed aircraft position from radar tracking data (O'Connor and Rutishauser 2001). These boundaries were represented by a series of cross-sectional "windows". The vortex behavior was determined at each window, and the required separation was determined by the altitude or location on the intended flight path that had the longest lasting wake vortex hazard (Hinton 1996). Only vortex encounters stronger than those of "operationally acceptable strength" were considered for the separation required. An exact definition of "operationally acceptable" remains a topic for discussion.

AVOSS was deployed in 1999 and 2000 at Dallas/Fort-Worth (DFW) International airport. The results indicated IFR throughput gains ranging from 0% to 16%, with an average gain of 6% (O'Connor and Rutishauser 2001). The upper limit on the gain of 16% was approximately equal to the difference between the default spacing and minimum runway occupancy time, indicating that wake vortex separation was no longer the bottleneck at that point.

The data from the DFW deployment was also used to validate the wake vortex models. In two out of three cases the minimum separation possible (limited by runway occupancy time) was recommended by AVOSS models, and these recommendations were not contradicted by sensor measurements. In 99% of examined cases, the observed wake hazard times did not exceed predictions, indicating that the reduced separation recommended by AVOSS could safely be applied. In the remaining 1% of cases, where wake hazard times did exceed the times predicted by AVOSS, they never exceeded the prediction by more than 20 seconds (5 seconds in half of the cases). This means that a possible wake vortex encounter could have occurred in those cases only if an aircraft had deviated significantly from the localizer or glide slope path, which was unlikely given the typical pilot performance (O'Connor and Rutishauser 2001).



Figure 1.1. An A320 landing in the background of the NASA lidar van (left) – Memphis International Airport, 1995. The AVOSS mission insignia (right).

Wake Vortex Scenarios Simulation (WakeScene) Package

The Wake Vortex Scenarios Simulation (WakeScene) Package was jointly developed by the Deutsches Zentrum für Luft- und Raumfahrt (DLR) and Airbus (Holzäpfel et al. 2009). The simulation software estimates the frequency and severity of wake vortex encounters using Monte Carlo simulations of both the departures and the arrivals of aircraft pairs. Wake vortex transport and decay models (with the option to choose between D2P, P2P, and APA) are used to predict wake vortex behavior. D2P (Deterministic Two Phase) and P2P (Probabilistic Two Phase) are fast-time wake models developed by DLR and APA (AVOSS Prediction Algorithm) is the DLR implementation of NASA’s wake model as reported in Robbins and Delisi (2002). The wake models provide vortex trajectories, time history of the circulation strength, and encounter angles within a series of computational gates. WakeScene uses the NOWcasting Wake VortexImpact Variables (NOWVIV) database which includes a full year of weather statistics for the Frankfurt airport. The NOWVIV system has undergone extensive validation tests using a wide range of meteorological sensors (Frech et al. 2007; Frech and Holzäpfel 2008).

The WakeScene package determines the relative wake vortex encounter probability (usually during the final approach on a single runway), and passes the relevant parameters of a potential wake vortex encounter to Vortex Encounter Severity Assessment (VESA) tool. VESA calculates the associated severity of the encounter (Holzäpfel et al. 2009) based on the aerodynamics, actual weights, and configurations of the aircraft types involved in the scenario. A flight-path deviation model is also used to determine the stochastic deviations of the aircraft from the nominal glide path. The applications of WakeScene have ranged from determining the wake vortex behavior for very large transport aircraft, re-categorizing of the wake turbulence separation minima, wake vortex advisory systems, sensitivity analyses, capacity optimization and the study of safety cases.

Wake4D

Wake4D is a wake vortex prediction platform, developed by the Université catholique Louvain (UCL) that uses meteorological input data as well as aircraft trajectory information to calculate the circulation strength of wake vortices in a discrete series of computational gates downwind of the generating aircraft (De Visscher et al. 2010). UCL’s Deterministic wake Vortex Model (DVM) and the probabilistic version (PVM) have been developed to predict wake vortex decay and transport in real-time. When set to the probabilistic mode, Wake4D generates envelopes of wake vortex locations using a Monte-Carlo type analysis.

The DVM model has been applied in several European projects such as the Aircraft Wing Advanced Technology Operations (AWIATOR), the Fundamental Research on Aircraft Wake Phenomena (FAR-Wake), and the Crosswind-Reduced Separations for Departure Operations (CREDOS). Wake4D can be

used for analyses as well as in real-time operational systems, e.g., as a part of an ATM system or for on-board wake vortex prediction and alert systems (De Visscher et al. 2010).

Wirbelschleppen- Vorhersage- und Beobachtungssystem (WSVBS)

The Wirbelschleppen- Vorhersage- und Beobachtungssystem (Wake Vortex Prediction and Monitoring System) was developed by DLR to study closely-spaced parallel runway operations in general and for Frankfurt airport in particular (Holzäpfel et al. 2009; Gerz et al. 2009). WSVBS provides weather dependent dynamic separations for either closely-spaced runways or single runway operations for weight class combinations and dynamic pairwise separations. WSVBS makes use of meteorological data obtained through a combination of a SODAR/RASS system and an ultrasonic anemometer in ground proximity. The numerical weather prediction system, NOWVIV is also employed to provide weather inputs (Frech et al. 2007; Frech and Holzäpfel 2008).

WSVBS uses DLR's P2P model to predict the upper and lower bounds on circulation strength and positions of generated wake vortices using 2σ -confidence intervals and incorporates the flight path adherence statistics (Holzäpfel et al. 2011). To determine the shape, size, and location of the keep-out region, WSVBS incorporates DLR's Simplified Hazard Area Prediction (SHAPE) model. In this model, the hazard area is defined in terms of the roll control ratio (RCR), which is the aileron deflection required to compensate the wake vortex induced roll moment as a fraction of the maximum aileron deflection (Schwarz and Hahn 2005). The RCR criterion is shown in Figure 1.2.

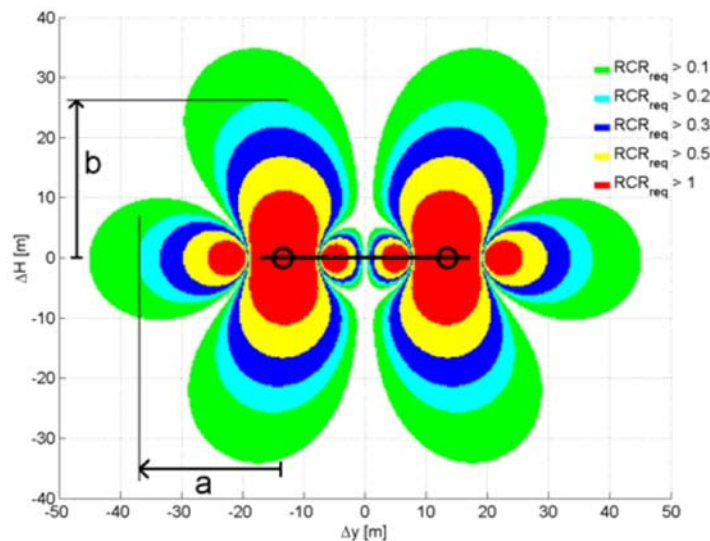


Figure 1.2. Roll control ratio as a function of distance to vortex axis. SHAPE uses a maximum of $RCR \leq 0.2$ for acceptable flight conditions, indicated by allowances 'a' and 'b' (Schwarz and Hahn 2005).

The final size and shape of the keep-out region is determined by adding a safety buffer to the vortex area prediction. In its current form, the WSVBS predicts wake vortex evolution for the final approach phase of flight, starting at the final approach fix (FAF), 11nmi before the touchdown zone, using thirteen computational gates (Holzäpfel et al. 2011). The spacing between the gates decreases with altitude, in order to properly account for ground effect. Lidar measurements are used to verify the predictions of the WSVBS at low altitude for the most critical gates (Holzäpfel et al. 2009).

WSVBS was evaluated at the Frankfurt Airport from December 2006 to February 2007. The WSVBS-derived separations were compared to a baseline of standard International Civil Aviation Organization (ICAO) separations. Although the demand exceeded capacity for both the ICAO and WSVBS separations, the WSVBS flow was able to closely follow demand while the ICAO flow accumulated delayed flights during the day. The reduced separations predicted by WSVBS could be used for 76.4% of the day. If the

real traffic mix and operational constraints for the same time period were taken into account the net capacity gain from using WSVBS was slightly larger than 3% (Gerz et al. 2009). In all investigated cases (1100 landings during 16 days) the recommended operation mode was correct, with no vortices detected in the flight corridor after the predicted minimum separation time (Gerz et al. 2009).

Wake Turbulence Re-Categorization Program

Under the current Federal Aviation Administration (FAA) regulations, the Air Traffic Control (ATC) imposes wake spacing standards for IFR aircraft based on maximum certified takeoff weight (FAA AC 90-23G). The separation standards and weight categories are listed in Tables 1-2. The B757 is in the “Large” weight category, but a special wake separation standard has been defined for it.

Table 1.1: FAA Wake Separation Standards (At the Threshold)

		Follower (Nautical Mile)				
		Super	Heavy	B757	Large	Small
Leader	Super	MRS	6	7	7	8
	Heavy	MRS	4	5	5	6
	B757	MRS	4	4	4	5
	Large	MRS	MRS	MRS	MRS	4
	Small	MRS	MRS	MRS	MRS	MRS

Table 1.2: Aircraft Weight Classes

Category	Weight
Heavy	MTOW \geq 300,000lbs
Large	41,000lbs < MTOW < 300,000
Small	MTOW \leq 41,000lbs

In addition to the “Heavy”, “Large”, and “Small” categories (Table 1.2), the “Super” category has been approved on an interim basis and currently consists of two aircraft – the Airbus A380 and the Antonov AN225.

To alleviate the capacity constraints imposed by the current wake separation standards, the FAA has suggested a phased approach to re-categorize the wake spacing standards. FAA’s Wake Re-categorization Program (RECAT) consists of three implementation phases:

- RECAT-I Static Six Category Separation
- RECAT-II Static Pair-wise Separation
- RECAT-III Dynamic Pair-wise Separation

New wake separation standards under RECAT-I (Tables 1.3-1.4) were recently introduced and are described in FAA Order JO 7110.659C. These standards are based on aircraft dynamics parameters (wingspan, final approach speed, and roll moment capability) in addition to the maximum takeoff weight (MTOW). The effort also took into account the traffic mix at five US (Atlanta, Newark, John F. Kennedy,

Chicago O’Hare, and San Francisco) and four European airports (Heathrow, Amsterdam, Frankfurt, and Charles de Gaulle) to further optimize the re-categorization. RECAT-I has been implemented at several airports with tremendous success. After the implementation at Memphis, FedEx reported an arrival rate improvement of 20%, savings of 3.3 minutes per flight in taxi-out time and 2.6 minutes per flight. Fuel savings have been on the order of 4.18 million gallons per year which translates to an annual reduction in carbon dioxide emission of 39,992 metric tons. Currently the work is underway on RECAT-II implementation which is expected to go into effect sometimes in 2016.

Table 1.3: RECAT-I Wake Separation Standards for On Approach

		Follower (Nautical Mile)					
		A	B	C	D	E	F
Leader	A		5	6	7	7	8
	B		3	4	5	5	7
	C				3.5	3.5	6
	D						4
	E						
	F						

Table 1.4: RECAT-I Weight Categories

Category	Weight	Wingspan
A	MTOW \geq 300,000lbs	$b_G > 245\text{ft}$
B	MTOW \geq 300,000lbs	$175\text{ft} < b_G \leq 245\text{ft}$
C	MTOW \geq 300,000lbs	$125\text{ft} < b_G \leq 175\text{ft}$
D	MTOW $<$ 300,000lbs <i>or aircraft with: $90\text{ft} < b_G \leq 125\text{ft}$</i>	$125\text{ft} < b_G \leq 175\text{ft}$
E	MTOW $>$ 41,000lbs	$65\text{ft} < b_G \leq 90\text{ft}$
F	MTOW $<$ 41,000lbs <i>or aircraft capable of a MTOW less than 15,500lbs regardless of wingspan, or a powered sailplane</i>	$b_G \leq 125\text{ft}$

FAA’s RECAT-I and RECAT-II development and implementations have relied primarily on wake vortex measurements obtained from pulsed lidars and other wake sensors. Although the work has not begun on RECAT-III, its eventual implementation would require modeling capabilities in order for aircraft to perform wake-based dynamic self-separation.

A Coupled Probabilistic Wake and Aircraft Response Prediction Model

NASA's AVOSS program was not only the pioneering effort but also the most comprehensive in its scope to develop wake vortex solutions for enhancing capacity and efficiency of terminal area operations. The program in its concept of operations used a combination of wake prediction models and wake sensors to dynamically space aircraft for the first time. Since then there have been several efforts to use wake solutions in the development of advanced air traffic management concepts. The fast-time models were used in the safety analysis of the Simplified Aircraft Based Paired Approach (SAPA). SAPA has been proposed for closely spaced parallel runway operations in IMC (Johnson, et al. 2013; Guerreiro et al. 2010). The use of NASA's wake models for ATM concepts development and safety analysis however has been limited. This is primarily because the research has remained focused on better characterization of wake vortex behavior under varying atmospheric conditions and on the development of deterministic wake prediction models.

The initial conditions of fast-time models (weather and aircraft parameters) can have large uncertainties (Holzäpfel 2014; Pruis and Delisi 2014), which makes their use for ATM applications difficult in the absence of any uncertainty quantification (Figure 1.3 – left panel). A probabilistic model on the other hand, takes into account the uncertainties in initial conditions and provides bounded solutions (Figure 1.3 – right panel). For ATM applications a bounded zone of wake hazard is required rather than point trajectories of vortices. Guerreiro et al. (2010) have used NASA's fast-time wake models in the Monte-Carlo sense for the safety analysis of the SAPA concept. Pruis and Delisi (2011b) have suggested an approach similar to the one described in this study but without any coupling to aircraft response models.

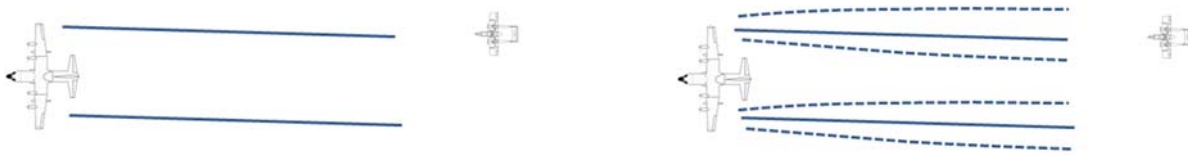


Figure 1.3. Deterministic (left) vs. probabilistic (right) wake vortex prediction. Probabilistic models can provide bounded wake hazard avoidance regions which are more applicable for designing ATM concepts and conducting safety analysis.

Another difficulty in using wake models for ATM applications has been the lack of wake hazard metric specification. Several wake encounter metrics have been proposed in the past (van der Geest 2012) but no standard has been defined to date. These metrics include the wake circulation strength, rolling moment coefficient, bank angle, and roll control ratio. In this study, the vortex-induced rolling moment coefficient (C_{lv}) is used to define the wake hazard metric. The circulation strength obtained from the fast-time wake models is converted to C_{lv} in order to provide an aircraft dependent hazard metric.

The focus of this study was on the development of a probabilistic wake vortex transport model that is coupled with an aircraft response model. In Section 2, a probabilistic wake vortex model is proposed and evaluated using data from two wake vortex field experiments. The wake hazard metric defined by Bowles and Tatnall (Tatnall 1995) is described and evaluated in Section 3. Section 4 provides an example application of the coupled probabilistic wake and aircraft response model and a summary is provided in Section 5.

2. Probabilistic Wake Vortex Modeling

A brief description of the deterministic fast-time wake models and the field experiment data used for validation is given in this section. The Monte-Carlo methodology for obtaining probabilistic bounds of wake location and strength is described in detail and the validation results using data from two different field experiments is provided.

Fast-Time Wake Vortex Decay and Transport Models

Fast-time wake vortex models have been developed for the real-time prediction of wake transport and decay based on aircraft parameters and ambient weather conditions. The aircraft dependent parameters include the initial vortex descent velocity (V_0), the vortex pair separation distance (b_0), and the position of the generating aircraft. The atmospheric initial conditions include vertical profiles of either temperature or potential temperature (θ), eddy dissipation rate (ϵ), and crosswind. The model output consists of time histories of circulation strength and location of point vortices (Figure 2.1). The models assume that all vorticity created due to lift is rolled up into a pair of counter-rotating vortices at the time of model initialization.

Various evaluations of the fast-time models have concluded that in general the errors in model circulation predictions have an average root mean square error on the order of $0.2\Gamma_0$ to $0.3\Gamma_0$ (Γ_0 is the initial wake circulation). The vertical transport errors are on the order of $0.5b_0$ and the lateral transport errors are on the order of b_0 (Pruis and Delisi 2011c; Feigh et al. 2012; Ahmad et al. 2014b). The lateral transport errors can be reduced to as low as $0.5b_0$ if more accurate crosswind initial conditions are provided to the fast-time models (Pruis et al. 2011a).

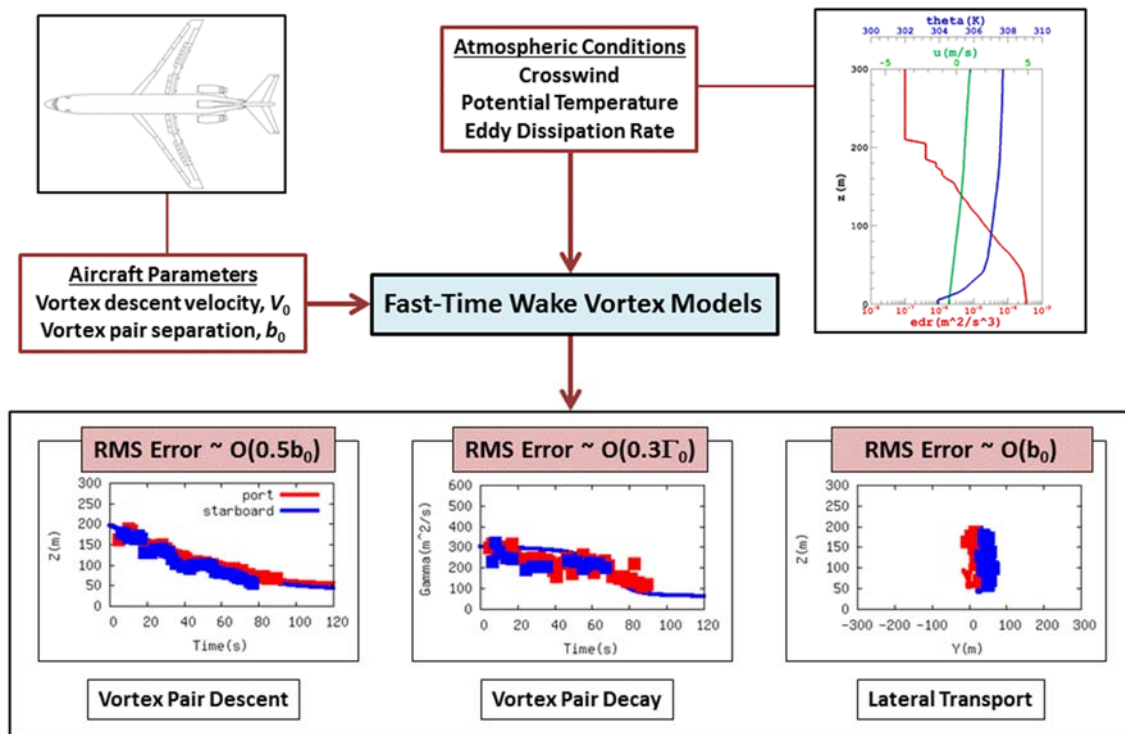


Figure 2.1. The flowchart shows the fast-time wake model inputs and outputs. The average root mean square errors (rmse) in the model prediction of vortex circulation strength and location are also given (Ahmad et al. 2014c).

The first fast-time wake transport and decay model was developed by Greene (1986). Some of the fast-time models currently in use include: AVOSS (Aircraft Vortex Spacing System) Prediction Algorithm (APA), TASS (Terminal Area Simulation System) Derived Algorithms for Wake Prediction (TDP), Deterministic 2-Phased (D2P), Probabilistic 2-Phased (P2P) model, and the Deterministic wake Vortex Model (DVM). The APA and TDP models have been developed by NASA, while the D2P and P2P models (Holzäpfel 2003) have been developed by DLR. The DVM (de Visscher et al. 2010) model has been developed by the Université catholique de Louvain (UCL). The AVOSS Wake Vortex Prediction Algorithm (Version 3.4) and the TASS Driven Algorithms for Wake Prediction (Version 2.1) were used in this study (Ahmad et al. 2014b).

AVOSS (Aircraft Vortex Spacing System) Prediction Algorithm (APA)

The development of the APA model was initiated during the AVOSS program (Perry et al. 1997; Hinton 2001). The model computes the out-of-ground-effect (OGE) decay and descent based on Sarpkaya (Sarpkaya 2000; Sarpkaya et al. 2001). The scheme to compute lateral vortex transport is based on the vertical profile of crosswind (Robins and Delisi 2002), and the in-ground-effect (IGE) transport accounts for vortex spreading and rebound (Corjon and Poinot 1996; Robins et al. 2002). The model has an algorithm for enhanced rate of decay during the ground effect developed by Proctor et al. (2000). The code development of APA model is described in Robins and Delisi (2002).

TASS (Terminal Area Simulation System) Driven Algorithms for Wake Prediction (TDP)

The TDP model (Proctor et al. 2006) has been developed from parametric studies using large eddy simulation (LES) of wake vortices (Proctor 1998; Proctor et al. 2000; Han et al. 2000). The parametric studies were conducted with the Terminal Area Simulation System (TASS) developed by Proctor (1987). The TDP model uses separate prognostic equations for vortex descent rate and circulation. The effect of crosswind shear on vortex descent rate is taken into consideration, which allows the modeling of vortex tilt due to crosswind (Proctor and Ahmad 2011). The mechanics of the in-ground-effect (IGE) model is the same as in APA. However, TDP transitions into near-ground effect (NGE) at a non-dimensional height, $Z^*= 1$, while APA's transition is at $Z^*= 1.5$. The response of the two models in NGE/IGE can be different since they do not enter these phases with the same decay rates. The bounding decay rates for TDP and APA are also different in the IGE phase.

Wake Vortex Field Experiments

Memphis 1995 Wake Vortex Field Experiment

A comprehensive field experiment to measure wake vortices and the associated ambient meteorological conditions was conducted at the Memphis International Airport in Memphis, Tennessee from August 6 through August 29, 1995 (Zak 1995; Campbell, et al. 1997). The wake data were collected using a continuous wave lidar. The meteorological sensors included radiosondes, sodars, a wind profiler, one 150ft high meteorological tower, a Radio Acoustic Sounding System (RASS), and NASA Langley's OV-10 research aircraft. The radiosondes were used to measure winds and temperature measurements (10s averages) at 50m vertical resolution. Temperature (5min averages) was measured using RASS every 30min at 14 vertical levels from 127m to 1492m. The 150ft (45.7m) meteorological tower was equipped with a large array of sensor systems. Winds, temperature and moisture were measured from the tower at different heights. Turbulence quantities (turbulence kinetic energy and eddy dissipation rate) were estimated from wind measurements at 5m and 40m heights. Additional meteorological data such as atmospheric pressure, temperature, etc. were obtained from the Surface Aerodrome Observations (SAO) and the Automated Surface Observations System (ASOS).

Denver 2006 Wake Vortex Field Experiment

The Denver 2006 Out of Ground Effect (OGE) field experiment was conducted during the months of April to June (Ahmad and Pruis 2015). The primary objective of this deployment was to track OGE vortices in lateral transport (large advection distances and longer time decay histories). In order to accomplish this objective, the lidar placement and configuration was such that the data collection focused on one direction of wake transport only (westerly winds). The meteorological measurements needed for inputs into the fast-time wake vortex models were obtained using an MTP5 (temperature profile) and directly from the pulsed lidar observations (crosswind and EDR profiles). Additionally, measurements of total wind, turbulence and temperature measurements were also obtained near the surface at three heights on a 106ft tall meteorological tower. The altitudes of the sensors were at 7m (23ft), 14.6m (48ft), and 32.3m (103ft) AGL.

Data Processed for Fast-Time Wake Models

Aircraft Data

The initial position (offset) of the vortex pair with respect to the runway centerline y_0 was estimated using an average of the first few data points for each landing. The initial height of the vortices z_0 was estimated from backward extrapolation of the altitude trajectory in time. The initial separation distance between the vortices b_0 was estimated assuming an elliptical wing loading,

$$b_0 = \frac{\pi}{4} b_G, \quad (2.1)$$

where b_G is the wingspan of the wake generating aircraft. The initial vortex descent rate was estimated from the aircraft weight, aircraft speed, air density, and the initial vortex separation b_0 ,

$$V_0 = \frac{W_G}{2\pi\rho V_G b_0^2}, \quad (2.2)$$

where g ($=9.81\text{m/s}^2$) is the acceleration due to gravity, ρ is the air density – which was assumed to be 1.2kg/m^3 for all the Memphis landings, V_G is the reported airspeed of the wake generating aircraft, and W_G is the reported landing weight of the wake generating aircraft.

In the case of Denver data, the density was assumed to be 1.02 kg/m^3 for all the landings. The airspeed (V_G), and the landing weight of the aircraft (W_G), were estimated from reference tables. Figure 2.2 shows the distribution of different wake category aircraft in the two datasets.

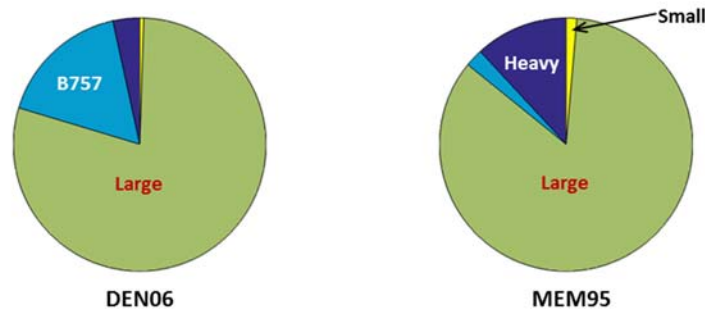


Figure 2.2. Distribution of the aircraft wake categories in the DEN06 dataset (left) and the MEM95 dataset (right).

Crosswinds

The profiles of the mean crosswind for the Memphis dataset were based on data fusion from several different wind sensors including the two Doppler radars, the meteorological tower, and the SODAR. For

the Denver data, crosswind profiles were estimated using the average of two horizontal in-plane wind estimates from the pulsed lidar, where one profile was estimated just prior to the aircraft passage and one profile was estimated just after the end of the wake observations.

Eddy Dissipation Rate

Vertical profiles of EDR for the Memphis dataset were estimated using the two sonic anemometers on the meteorological tower and extrapolating to heights using similarity theory (Han et al. 2000). Turbulence profiles were extrapolated to the ground and to a height above the observed vortices with a constant EDR value whenever the measured profiles did not extend to those heights. For the Denver data, the vertical profiles of EDR were generated using the lidar data (Pruis et al. 2013). Figure 2.3 shows the distribution of non-dimensional eddy dissipation rates in the two datasets categorized by turbulence intensity.

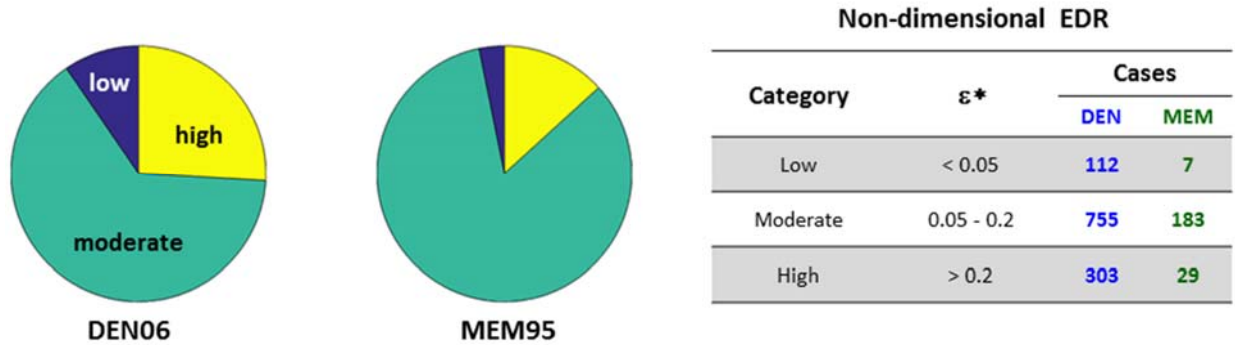


Figure 2.3. Distribution of non-dimensional eddy dissipation rates (ϵ^*) in the Denver (DEN06) and Memphis (MEM95) datasets. $\epsilon^* = (\epsilon b_0)^{1/3} V_0^{-1}$.

Stratification

Temperature profiles for the Memphis dataset were estimated using a fusion of the RASS and temperature sensors on the ASOS and the meteorological tower. The temperature profiles were converted to potential temperatures using the dry adiabatic lapse rate. The highest temperature measurement on the tower was at approximately 43m AGL and the lowest observation of the RASS was at 127m. For Denver, the MTP5 microwave radiometer was used to estimate temperature up to a height of 600m with one measurement every 50m above the sensor. These temperature estimates were converted to potential temperature using a dry adiabatic lapse rate (0.00976K/m). Figure 2.4 shows the distribution non-dimensional Brunt-Väisälä frequency in the two datasets categorized by the level of stratification.

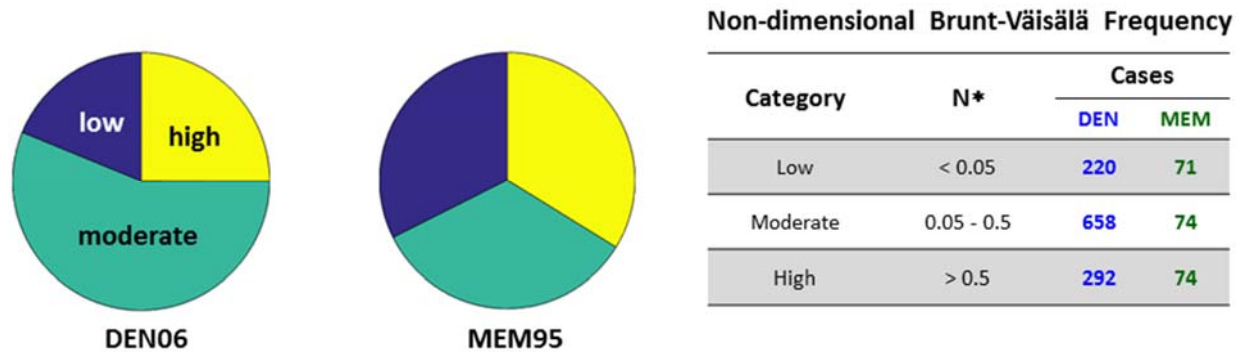


Figure 2.4. Distribution of non-dimensional Brunt-Väisälä frequency (N^*) in the Denver (DEN06) and Memphis (MEM95) datasets. $N^* = N b_0 V_0^{-1}$.

Monte Carlo Simulation Methodology

The Monte-Carlo simulation methodology used in this study is described in detail in this section using examples from the Memphis 95 dataset. The methodology is evaluated using NASA's Memphis 95 and Denver 06 wake vortex datasets.

The model initial conditions which can be perturbed include: ε , θ , u , b_0 , V_0 , z_0 , and y_0 . If the probability density functions (pdf) are available, then they are utilized, otherwise uniform distributions are used within prescribed bounds. The pdfs are generated by binning the input variable into a density histogram. Various distributions can be fitted using the maximum likelihood estimation method. The Kolmogorov-Smirnov test is then applied to determine the best distribution for the data,

$$D^* = \max_x \left| \hat{F}(x) - G(x) \right|, \quad (2.3)$$

where $\hat{F}(x)$ is the empirical cumulative distribution function and $G(x)$ is the tested continuous distribution. In case a varying vertical profile is used, then the profile is truncated at z_0 (height of vortex generation) and the mean is calculated from ground to z_0 . Once the averages have been calculated, k perturbations are generated using the probability density functions. Uniform weather profiles are generated from these perturbations. Simulations are performed with all inputs, and the standard deviation and the mean are calculated for each time step. The standard deviation is then added and subtracted to the mean to create bounds for circulation strength and vortex location.

Generation of Initial Conditions

A constant value of hundred bins was used to find the pdf for eddy dissipation rates (EDR). Figure 2.5 (left panel) shows all the EDR profiles for Memphis 95 dataset and the EDR histogram is shown in the right panel. The histogram shows a large spike in the lowest bin. This is because of the large number of zeros for EDR in the Memphis dataset. The null values of EDR were replaced with an EDR value of $10^{-7} \text{ m}^2/\text{s}^3$. The histogram is normalized such that the surface of the histogram is equal to one.

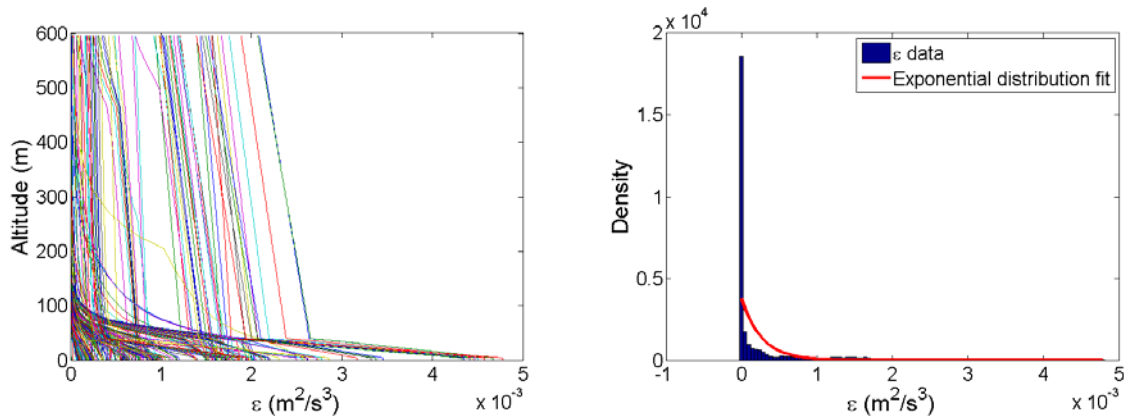


Figure 2.5. Memphis '95 EDR profiles (left panel) and the EDR histogram with the exponential distribution fit (right panel).

Multiple distributions were fitted using the maximum likelihood estimation method. The different distributions were then subjected to Kolmogorov-Smirnov test to find the best fit. For EDR this resulted in an exponential distribution, with $\mu = 2.654 \times 10^{-4} \text{ m}^2/\text{s}^3$. The pdfs can also be generated using simulation data

from mesoscale models (Ahmad and Proctor 2012). The National Weather Service (NWS) provides turbulence forecasts as part of their aviation products.

The distribution for crosswind was generated using the same methodology. First, the data was binned and, then using the Kolmogorov-Smirnov test, the best fitting distribution was determined (Figure 2.6). A logistic distribution was the best fit to the data, with the mean, $\mu = -0.4327\text{m/s}$, and the standard deviation, $\sigma = 1.4815\text{m/s}$.

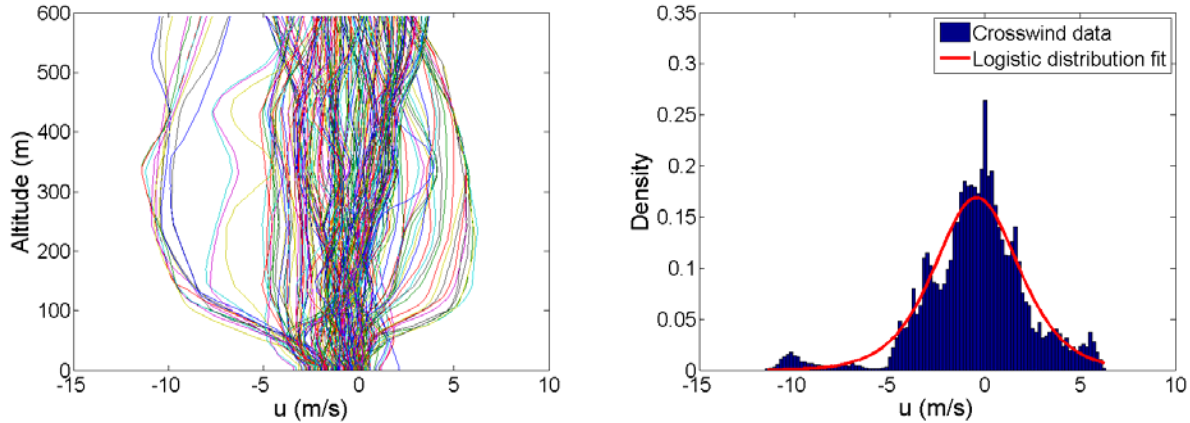


Figure 2.6. Memphis '95 crosswind profiles (left panel), and the crosswind histogram with logistic distribution fit (right panel).

The uncertainty in crosswind can also be quantified in terms of the deviation from the mean. Using information from the current wind profile, for example an inflight measurement, the crosswind distribution can be estimated with smaller bounds. This is done by using a normalized probability density function. The normalization is done with respect to the profile mean. Figure 2.7 shows a schematic of this method. By translating the profiles such that their mean is zero, the data distribution represents the deviation of the crosswind from the mean value. Figure 2.8 shows the normalized pdf for the crosswinds. The best fitting distribution was the logistic distribution with mean, $\mu = 0.0259\text{m/s}$, and standard deviation, $\sigma = 0.582\text{m/s}$. Comparing the normalized pdf with the full pdf it can be seen that the standard deviation is significantly smaller for the normalized pdf which increases the confidence bounds.

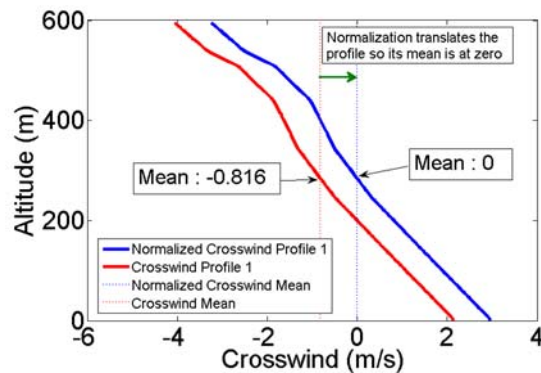


Figure 2.7. Schematic showing the normalization of crosswind profile.

Perturbations in the crosswind initial conditions can also be generated using different methods. Uniform distributions can be defined as well as fixed levels within prescribed bounds. Holzäpfel (2014) suggested using normal distributions for crosswinds ($2\sigma = 2.5\text{-}3.8\text{m/s}$) based on the uncertainty of the onboard measurements. Ahmad et al. (2014c) used this methodology with the mean set to the average crosswind

measured during NASA's Wallops flight tests (Vicroy et al. 1998) with favorable results. The crosswind pdf can also be generated using data from numerical weather prediction models.

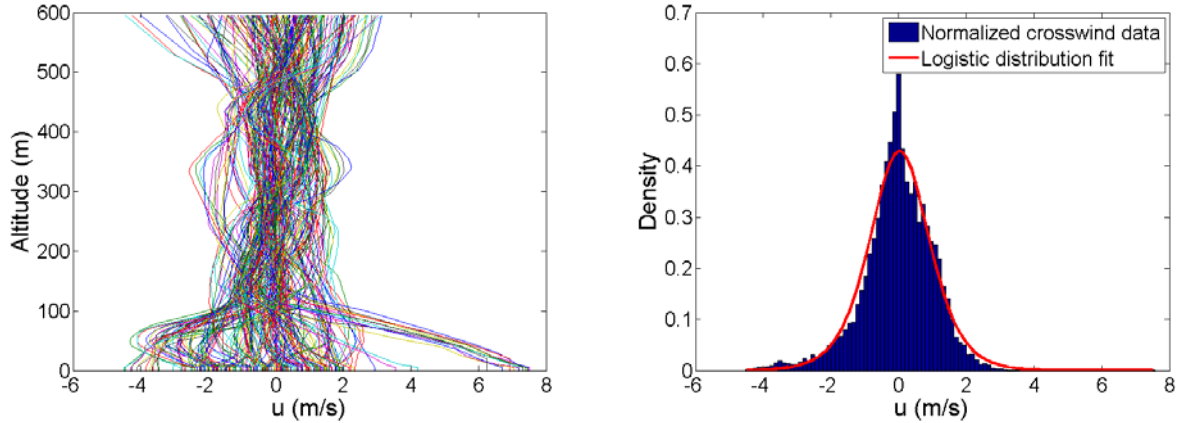


Figure 2.8. Memphis '95 normalized crosswind profiles (left panel) and the normalized histogram with the logistic distribution fit (right panel).

The atmospheric stability is given by the Brunt-Väisälä frequency

$$N = \sqrt{\frac{g}{\theta} \frac{d\theta}{dz}}, \quad (2.4)$$

where θ is the potential temperature, and g is the acceleration due to gravity. The initial conditions for the wake models are either in terms of potential temperature or temperature. If temperature data is provided then it is converted to potential temperature using the adiabatic lapse rate. Since it is the gradient of the potential temperature which is the measure of atmospheric stability and affects the wake circulation decay, the perturbations in potential temperature are based on the potential temperature gradient, $d\theta/dz$. The probability density functions generated, are therefore also for the potential temperature gradient.

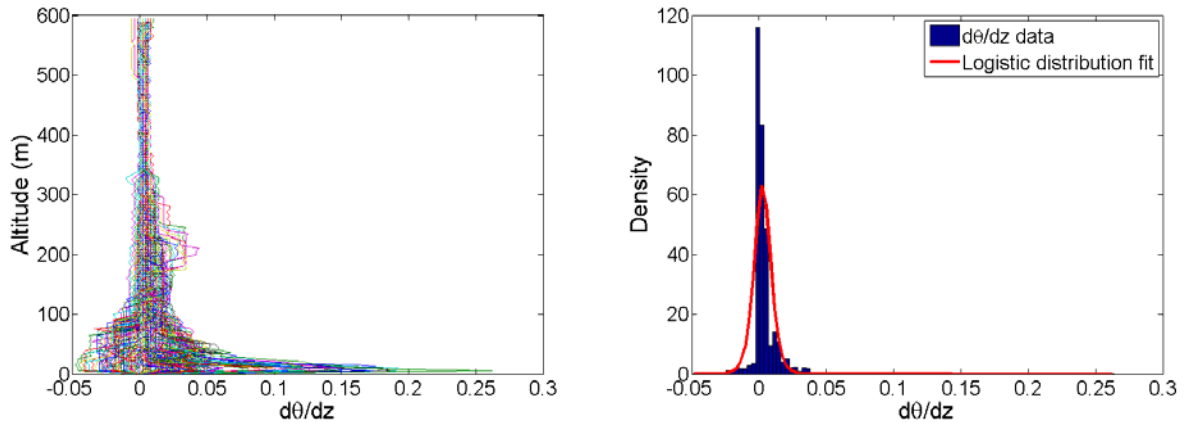


Figure 2.9. Memphis '95 potential temperature gradient profiles (left panel) and the potential temperature gradient histogram with logistic distribution fit (right panel).

In Figure 2.9 the potential temperature gradient profiles and the histogram are shown. The best fitting distribution was the logistic distribution, with mean $\mu = 0.0027\text{K/m}$, and standard deviation, $\sigma = 0.004\text{K/m}$. Normalization of the potential temperature gradient was done in the same manner as for the crosswind. The best fitting distribution was again the logistic distribution, with mean $\mu = -0.0011\text{K/m}$, and standard

deviation, $\sigma = 0.0039\text{K/m}$ (Figure 2.10). In practice, the potential temperature profiles can be generated from mesoscale weather prediction models. Ahmad et al. (2013) showed that the stratification predictions from the mesoscale models compared well with observations and the model forecasts could be used for generating initial conditions for the wake models.

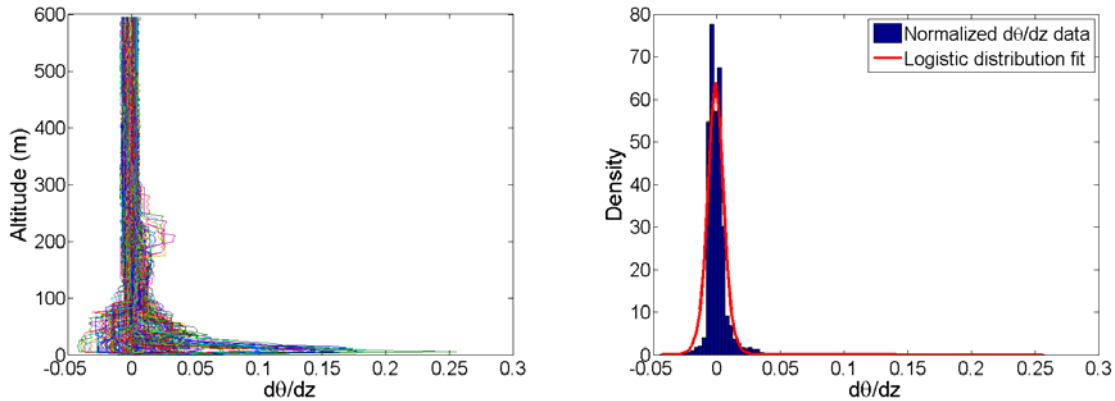


Figure 2.10. Memphis '95 normalized potential temperature gradient profiles (left panel) and the normalized potential temperature gradient histogram with the logistic distribution fit (right panel).

Distributions for aircraft specific initial conditions, y_0 , z_0 , V_0 , and b_0 were based on Holzäpfel (2014). The initial conditions for y_0 , and z_0 were estimated using normal distributions with mean set to y_0 and standard deviation set to 25m for lateral position and z_0 as the mean and the standard deviation set to 7m for the vertical position of the vortex pair. For the IGE cases the standard deviation is set to 4m in the vertical. The initial vortex circulation strength is varied from $0.9\Gamma_0$ to $1.25\Gamma_0$ based on the uncertainties in aircraft weight (Holzäpfel 2014). The initial descent velocity of the vortices as a function of Γ_0 is given by

$$V_0 = \frac{\Gamma_0}{2\pi b_0} \quad (2.5)$$

Holzäpfel (2014) pointed out that the assumption of elliptical wing loading for determining b_0 may not be valid for many aircraft configurations where it can be as low as $0.95b_0$. Given this uncertainty, a uniform distribution was used for the initial vortex separation distance bounded between $0.95b_0$ and b_0 . Figure 2.11 shows the initial conditions for eddy dissipation rate, crosswind, and potential temperature for a MEM95 case. The vertical profiles are truncated at the altitude of vortex initialization, z_0 in the calculation of averages.

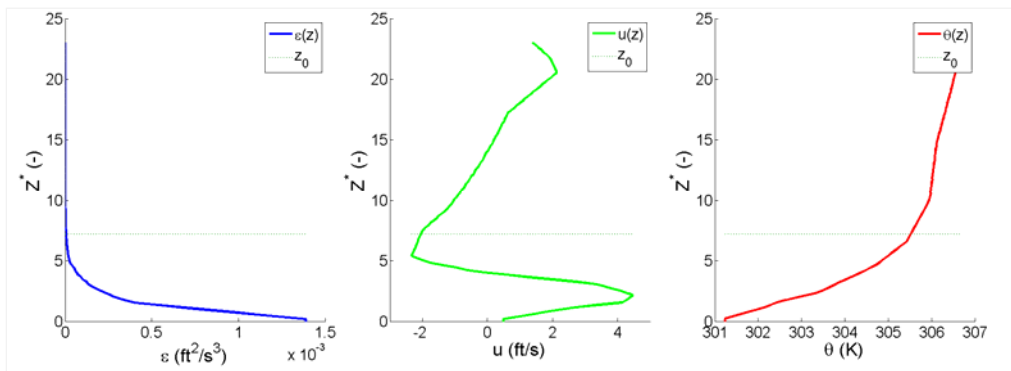


Figure 2.11. EDR (left), crosswind (center) and potential temperature (right) profiles from one of the Memphis cases. The horizontal dashed line denotes the height of vortex initialization and the data above it is not used in the generation of mean quantities.

Once the averages have been calculated for a case, k perturbations are generated using the pdfs described earlier. Constant profiles of eddy dissipation rate, crosswind, and potential temperature are generated from these perturbations (Figure 2.12). In the case of potential temperature, the random perturbations are generated based on the pdf of the potential temperature gradient. The potential temperature profile in the vertical is then calculated as follows

$$\theta(z) = \theta_0 + \frac{d\theta}{dz} \cdot z \quad (2.6)$$

where, θ_0 is the base state potential temperature set to 300K. Figure 2.13 shows the results of APA3.4 for the initial conditions in Figure 2.12.

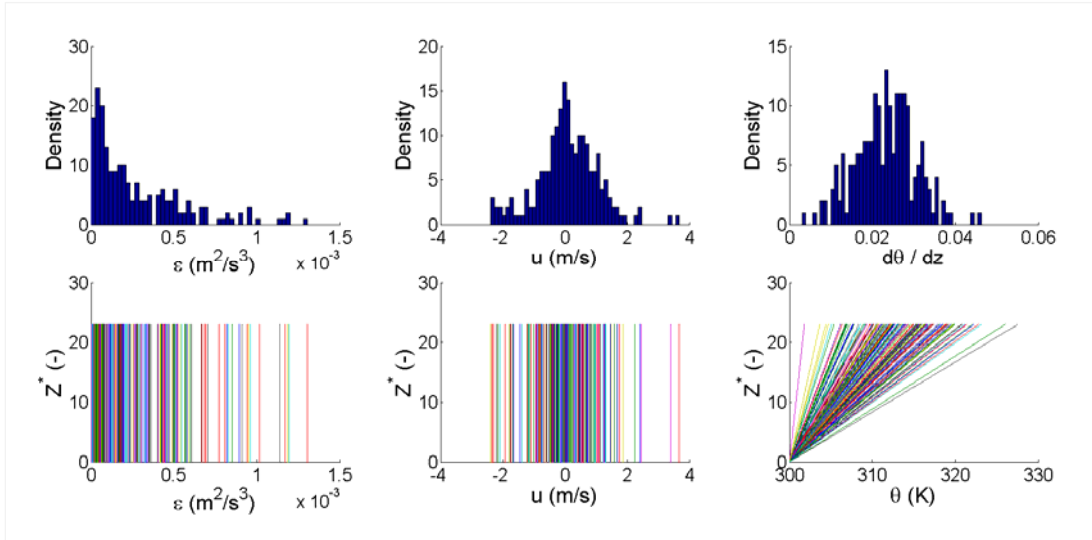


Figure 2.12. Top panel shows the probability density functions. Perturbations in the initial condition of eddy dissipation rate, crosswind, and potential temperature are shown in the bottom panel.

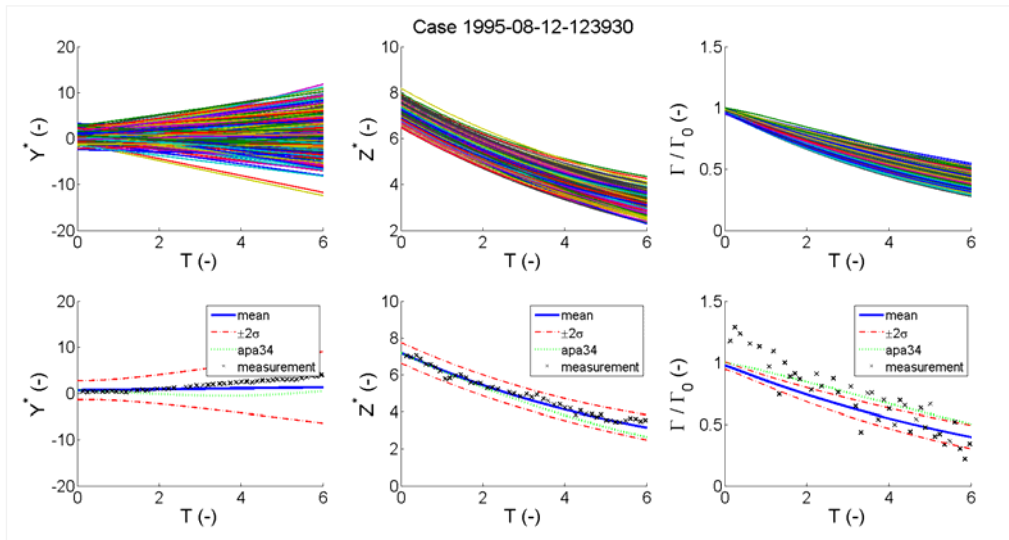


Figure 2.13. Results for a case from the Memphis '95 dataset using the APA3.4 model. The top row shows the results from all simulations. The bottom row shows the mean, and the $\pm 2\sigma$ bounds generated from the Monte-Carlo run.

The standard deviation and the mean are calculated at each time step in the of the vortex descent, transport, and decay time history

$$\sigma = \left[\frac{1}{n-1} \sum_{i=1}^n (x_i - \bar{x})^2 \right]^{1/2} \quad (2.7)$$

The standard deviation is then added and subtracted to the mean in order to create the $\pm\sigma$ and $\pm 2\sigma$ bounds. Figure 2.14 shows the bounds, and the mean, along with the lidar measurements. The deterministic output of APA3.4 and TDP2.1 models is also shown. The left panel shows results of Monte-Carlo simulations using only APA3.4 and the middle panel shows the results when using only TDP2.1 model. For the simulation result shown in the right panel, the mean and the bounds were generated using the output of both APA3.4 and TDP2.1 models.

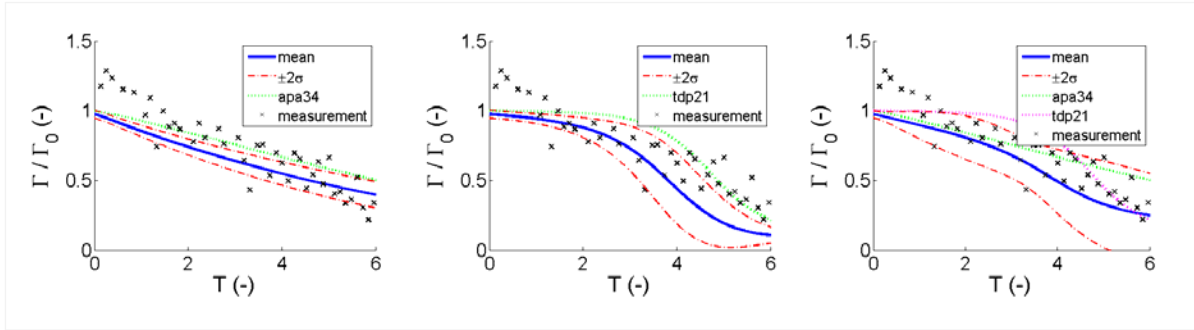


Figure 2.14. Circulation decay prediction. APA3.4 (left); TDP2.1 (center); and the multi-model ensemble of APA3.4 and TDP2.1 (right).

Simulation Results

The Monte Carlo method was evaluated using the Memphis 1995 and Denver 2006 datasets. To determine the success rate of the Monte-Carlo simulation, the number of lidar measurements which were bounded within the $\pm 2\sigma$ region were counted and divided by the total number of measurements in the case. For circulation strength, an additional metric was defined which looked at the lidar measurements bounded by the 2σ curve. Success rates for Memphis 1995 are given in Table 2.1. In general, the lateral transport was predicted with good accuracy (success rate of 99%). Prediction of vortex descent had a success rate in the range of 60%. TDP2.1 gave slightly better results than the APA3.4 for circulation decay predictions. Circulation success rates were much higher when using the upper bounds criteria. The multi-model ensemble consisting of APA3.4 and TDP2.1 improved the accuracy of the results for all parameters. In the case of circulation prediction, several observation are outside the predicted 2σ bounds (Figure 2.14). It should be noted that most of these circulation values are greater than the value of Γ_0 that was used to initialize the model.

Table 2.1: Success rates for models (MEM95)

Parameter	APA3.4	TDP2.1	Multi Model
y	0.99	0.99	0.99
z	0.60	0.63	0.63
$\Gamma_{\text{within bounds}}$	0.21	0.25	0.42
$\Gamma_{\text{under max}}$	0.44	0.59	0.61

The Denver 2006 evaluation results are given in Table 2.2. The lateral transport had a success rate of 97% for both models and the multi-model ensemble. The values for the vertical descent prediction were also similar to Memphis simulations and in the range of 60%. There was a significant improvement in circulation prediction when comparing the results of Memphis and Denver simulations. One reason for this difference could be due to different wake sensors used in the two field experiments. A continuous wave lidar was used in Memphis, whereas the Denver deployment used a pulsed lidar.

Table 2.2: Success rates for models (DEN06)

Parameter	APA3.4	TDP2.1	Multi Model
y	0.97	0.97	0.97
z	0.61	0.61	0.62
$\Gamma_{\text{within bounds}}$	0.50	0.41	0.51
$\Gamma_{\text{under max}}$	0.95	0.95	0.96

A sensitivity test was done to quantify the effect of the uncertainties in b_0 and Γ_0 (Figure 2.15). The effect of including the uncertainty in b_0 was much smaller than the effect of initial circulation strength. The success rates for APA3.4 with $0.9\Gamma_0$ to $1.25\Gamma_0$ bounds are given in Table 2.3 and show a marked improvement in the circulation prediction success rates and also improve the overall multi-model ensemble predictions. In this simulation, perturbations of Γ_0 were not used in TDP2.1 simulations.

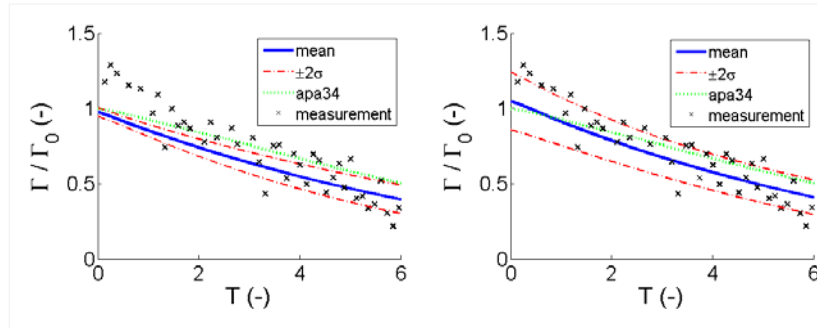


Figure 2.15. APA3.4 circulation decay results for a Memphis case using different types of model initializations. Perturbations in the vortex separation distance (left) and in the initial circulation strength (right).

Table 2.3: Success rates for models (MEM95) APA3.4 – V_0 [0.9-1.25]

Parameter	APA3.4	TDP2.1	Multi Model
y	0.98	0.99	0.99
z	0.68	0.63	0.72
$\Gamma_{\text{within bounds}}$	0.51	0.25	0.65
$\Gamma_{\text{under max}}$	0.70	0.59	0.81

3. Aircraft Response Modeling

A brief description of various vortex-induced hazard metrics which have been proposed in the past is given in this section. The Bowles-Tatnall method for calculating the vortex-induced rolling moment coefficient (Tatnall 1995) was used in this study and is described in detail.

Vortex Encounter Metrics

Ideally a wake hazard metric should be used that is generally accepted and for which a criterion (maximum/boundary value) can be set. It is important for this metric to have a strong relation with the actual encounter severity and thus is proportional to it. Another important characteristic is that the metric should be aircraft independent in order to set a boundary that is valid for every aircraft type. Some wake encounter hazard metrics which have been suggested in the past are:

- vortex circulation strength, Γ
- aircraft roll angle, Φ
- roll moment coefficient, C_{l_v}
- roll control ratio (RCR)

Vortex Circulation Strength

The vortex circulation strength is the easiest to implement since it is the direct output of the fast-time models. However, the aircraft response may not be directly deducible from its magnitude as it depends on several aircraft characteristics. Hallock et al. (2015) have proposed the calculation of roll moment coefficient (RMC) based on circulation strength using the following approximation

$$RMC = \frac{\Gamma}{V_F b_F}, \quad (3.1)$$

where Γ is the circulation strength of the generating aircraft's wake, V_F , and b_F are the speed and the wingspan of the follower aircraft.

Rolling Moment Coefficient

The vortex induced rolling moment coefficient, C_{l_v} is the normalized form of the rolling moment and is therefore aircraft independent. It requires aircraft parameters that are relatively easy to obtain such as the wing span and the wing planform area. Lang et al. (2010) noted that, "rolling moment coefficients of 0.05 to 0.07 are the maximum that can be controlled by the roll control authority of an aircraft using ailerons only, and that larger rolling moments might exceed an aircraft's roll control authority." The vortex induced rolling moment coefficient is given by

$$C_{l_v} = \frac{l_v}{\bar{q} S_F b_F}, \quad (3.2)$$

where l_v is the vortex-induced rolling moment, \bar{q} is the freestream dynamic pressure, and S_F is the following aircraft's wing planform area.

Roll Angle

The roll angle (bank angle) indicates the actual rotation of the encountering aircraft. It is an aircraft dependent metric and therefore different for every aircraft type. It also depends on the pilot response to the wake encounter which will be different for different pilots.

Roll Control Ratio

The Roll Control Ratio (RCR) is the ratio of the rolling moment coefficient and the available control power

$$RCR = \frac{C_{l_v}}{C_{l_{\delta a}} \cdot \delta_{a,\max}}, \quad (3.3)$$

where C_{l_v} is the vortex induced rolling moment of the encountering aircraft, $C_{l_{\delta a}}$ the aileron effectiveness coefficient and $\delta_{a,\max}$ is the maximum aileron deflection.

The criterion on the RCR can be set such that there is not only enough control to overcome the vortex-induced rolling moment but also to let the aircraft return to its normal attitude (Rossow, 1999). In practice, it is difficult to acquire data for the aileron effectiveness coefficient and the maximum aileron deflection (roll control) for different aircraft (van Baren, et al., 2011).

Bowles-Tatnall Method

The aircraft response to a wake vortex encounter is determined using the method developed by Bowles and Tatnall (Tatnall 1995). The method uses an idealized vortex model coupled with aerodynamic strip theory to calculate the response of the encountering aircraft. The method was selected because it is described in open literature and has undergone extensive validation. The vortex circulation strength is a primary input for the method which makes it straightforward to integrate it with the fast-time wake models. The net vortex-induced rolling moment coefficient is given by

$$C_{l_v} = \frac{2C_{L_G} C_{L_{\alpha F}} V_G b_G^2}{\pi^2 (AR)_G b_F^2 (1 + \lambda_F) V_F} \int_{-b_F/2b_G}^{b_F/2b_G} \left\{ \left[\bar{y} \left(1 - \frac{2b_G(1 - \lambda_F)}{b_F} |\bar{y}| \right) \right] \cdot \left[\left(\frac{\bar{y} + (\bar{Y}_F + \bar{s}) \cos(\Phi) + \bar{Z}_F \sin(\Phi)}{\bar{y}^2 + \bar{y}(2(\bar{Y}_F + \bar{s}) \cos(\Phi) + 2\bar{Z}_F \sin(\Phi)) + ((\bar{Y}_F + \bar{s})^2 + \bar{Z}_F^2 + \bar{r}_c^2)} \right) - \left(\frac{\bar{y} + (\bar{Y}_F - \bar{s}) \cos(\Phi) + \bar{Z}_F \sin(\Phi)}{\bar{y}^2 + \bar{y}(2(\bar{Y}_F - \bar{s}) \cos(\Phi) + 2\bar{Z}_F \sin(\Phi)) + ((\bar{Y}_F - \bar{s})^2 + \bar{Z}_F^2 + \bar{r}_c^2)} \right) \right] \right\} d\bar{y} \quad (3.4)$$

where, C_{L_G} is the lift coefficient of the generator, $C_{L_{\alpha F}}$ is the three-dimensional lift-curve slope of the follower, V_F and V_G are the airspeeds of the follower and the generator respectively, b_F and b_G are the wingspans of the follower and generator respectively. $(AR)_G$ is the wing aspect ratio of the generator, λ_F is the wing taper ratio of the follower, s is the half of vortex pair separation (b_0), r_c is the vortex core radius size, Φ is the bank angle of the follower, and (Y_F, Z_F) is the follower's center of gravity in inertial coordinates. The overbar symbol (e.g., \bar{y}) implies normalization by the generator wingspan, b_G .

Eq. (3.4) can be re-written by substituting

$$\Gamma_0 = \frac{2C_{L_G} b_G V_G}{\pi (AR)_G}, \quad (3.5)$$

where Γ_0 is the circulation strength of the generator's wake vortex

$$C_{l_v} = \frac{\Gamma_0 C_{L_{\alpha F}} b_G}{\pi b_F^2 (1 + \lambda_F) V_F} \int_{-b_F/2b_G}^{b_F/2b_G} \left\{ \left[\bar{y} \left(1 - \frac{2b_G(1-\lambda_F)}{b_F} |\bar{y}| \right) \right] \bullet \left[\begin{array}{l} \left(\frac{\bar{y} + (\bar{Y}_F + \bar{s}) \cos(\Phi) + \bar{Z}_F \sin(\Phi)}{\bar{y}^2 + \bar{y} (2(\bar{Y}_F + \bar{s}) \cos(\Phi) + 2\bar{Z}_F \sin(\Phi)) + ((\bar{Y}_F + \bar{s})^2 + \bar{Z}_F^2 + \bar{r}_c^2)} \right) \\ - \left(\frac{\bar{y} + (\bar{Y}_F - \bar{s}) \cos(\Phi) + \bar{Z}_F \sin(\Phi)}{\bar{y}^2 + \bar{y} (2(\bar{Y}_F - \bar{s}) \cos(\Phi) + 2\bar{Z}_F \sin(\Phi)) + ((\bar{Y}_F - \bar{s})^2 + \bar{Z}_F^2 + \bar{r}_c^2)} \right) \end{array} \right] \right\} d\bar{y} \quad (3.6)$$

The integrals in Eq. (3.4) and (3.6) assume a constant lift distribution across the wingspan and can be solved analytically. The analytical solution is given by

$$C_{l_v} = K_{l_v} (I_1 - I_2), \quad (3.7)$$

where,

$$K_{l_v} = \left(\frac{\Gamma_0}{\pi} \right) \left(\frac{C_{L_{\alpha F}} b_G}{b_F^2 V_F} \right) \left(\frac{1}{1 + \lambda_F} \right). \quad (3.8)$$

I_1 and I_2 are defined as follows:

$$I_i = \frac{1}{2} \left[(C_i^2 - A_i^2) \Omega - C_i \right] \ln \left[\frac{C_i^2 + A_i^2}{(C_i - B)^2 + A_i^2} \right] + \frac{1}{2} \left[(C_i^2 - A_i^2) \Omega - C_i \right] \ln \left[\frac{C_i^2 + A_i^2}{(C_i + B)^2 + A_i^2} \right] + A_i \left[4C_i \Omega \tan^{-1} \left(\frac{C_i}{A_i} \right) + (1 - 2C_i \Omega) \tan^{-1} \left(\frac{C_i - B}{A_i} \right) - (1 + 2C_i \Omega) \tan^{-1} \left(\frac{C_i + B}{A_i} \right) \right] \quad i=1,2 \quad (3.9)$$

The parameters, C_1 , C_2 , A_1 , A_2 , B , and Ω in the above equations are defined as follows:

$$C_1 = (\bar{Y}_F + \bar{s}) \cos(\phi) + \bar{Z}_F \sin(\phi), \quad (3.10)$$

$$C_2 = (\bar{Y}_F - \bar{s}) \cos(\phi) + \bar{Z}_F \sin(\phi), \quad (3.11)$$

$$A_1^2 = [(\bar{Y}_F + \bar{s}) \sin(\phi) - \bar{Z}_F \cos(\phi)]^2 + \bar{r}_c^2, \quad (3.12)$$

$$A_2^2 = [(\bar{Y}_F - \bar{s}) \sin(\phi) - \bar{Z}_F \cos(\phi)]^2 + \bar{r}_c^2, \quad (3.13)$$

$$B = \frac{b_F}{2b_G}, \quad (3.14)$$

$$\Omega = \frac{1 - \lambda_F}{B}. \quad (3.15)$$

The overbar symbol implies normalization by the generator wingspan, b_G , e.g., $\bar{Z}_F = \frac{Z_F}{b_G}$. The derivation of the method is given in Tatnall (1995) and also provided in Appendix A.

Evaluation using Wind Tunnel Data

The Bowles-Tatnall method is evaluated using wind tunnel data in this section. The wind tunnel experiment was performed in the 80ft x 120ft tunnel at NASA Ames Research Center (Rossow 1994).

A 3% B747-400 scale model was used to generate wake vortices and different types of wings were placed behind the generator to measure vortex encounters in terms of induced lift and induced rolling moment coefficient. The generating model was mounted upside-down to minimize the interference of the strut's wake on the wake vortices. Measurements of the encountered rolling moment were taken from the sting mounted on a vertical lift mechanism. This lift mechanism was attached to a tower that could be traversed in the lateral direction on a rail. By changing the following wing's lateral location the change of the rolling moment coefficient along the wing span direction could be estimated. The wind tunnel test conditions and the generating aircraft properties that are used are given in Tables 3.1-3.2. The properties of follower wings (numbered 1, 4, and 5) are given in Table 3.3.

Bowles-Tatnall method as described in Tatnall (1995) uses the idealized Burnham-Hallock vortex model with a core radius size of 6% of the wingspan. Various estimates for the core radius size, ranging from 1% to 7% of the wingspan have been suggested in literature (Delisi et al. 2003). Burnham and Hallock (2013) have reported a vortex core radius size of 5% of wingspan for a B747-100 based on field measurements. A sensitivity analysis was performed to assess the effect of different core radius sizes. Figures 3.2-3.4 show the comparison of C_{lv} calculation with the wind tunnel data for three different core radius sizes (2%, 4%, and 6% of the wingspan).

A clockwise rotation was set to be positive, which implies that the port vortex produced a positive rolling moment coefficient. This can be seen in the figures – the left peak shows positive C_{lv} values and the right peak negative values. Please note that the peaks in the plot for Wing 1 are inverted in Tatnall (1995) because the wing was inverted in that test. For consistency, the peaks have been kept in the same direction in all figures in this section.

In general, the method performed well when compared with measurements. The C_{lv} values are over-estimated at smaller core radii but for $r_c = 6\%$ the errors were low, especially for Wings 1, and 4.

Table 3.1: Wind Tunnel Test Conditions (Rossow 1994; Tatnall 1995)

Freestream dynamic pressure	20 lb/ft ²
Freestream velocity	131 ft/s

Table 3.2: Generator Parameters (Rossow 1994; Tatnall 1995)

Aircraft model type	B747-400
Wing Span	5.875 ft
Wing Area	4.94 ft ²
Aspect Ratio	6.96
Lift Coefficient (C_L) during tests	1.2

Table 3.3: Follower Parameters (Rossow 1994; Tatnall 1995)

Wing	Wing Span (ft)	Wing Area (ft ²)	Aspect Ratio	Taper Ratio	$C_{L\alpha}$ (rad ⁻¹)
1	1.093	0.220	5.44	1.00	4.050
4	2.998	1.283	7.00	0.31	4.300
5	6.003	5.100	7.06	0.30	4.300

The errors were also quantified in terms of root mean square error ($Error_{rms}$), mean absolute error ($Error_{mae}$), and bias in the model predictions

$$Error_{rms} = \sqrt{\frac{1}{n} \sum_{i=1}^n (x_i^{model} - x_i^{obs})^2}; \quad Error_{mae} = \frac{1}{n} \sum_{i=1}^n |x_i^{model} - x_i^{obs}|; \quad Bias = \frac{1}{n} \sum_{i=1}^n (x_i^{model} - x_i^{obs}) \quad (3.16)$$

Results of the error analysis are given in Table 3.4. A Burnham-Hallock model was used to characterize the vortex flow field with the core radius size of 6% in these calculations.

Table 3.4: Bowles-Tatnall Method

Wing	C_{lv}		
	rmse	mae	bias
1	0.0173	0.0101	0.0006
4	0.0086	0.0075	0.0034
5	0.0142	0.0123	0.0031

Correction to the Bowles-Tatnall Method

Bowles-Tatnall method described in the previous section over-estimates the C_{lv} . Although the estimate is conservative and provides a safety buffer, Bowles (2014) suggested a correction to the method that gives more accurate values of C_{lv} and is also consistent with the underlying physics of the problem. The overestimation of C_{lv} can be attributed to the assumption of a constant wing loading over the wing span – the wing lift-curve slope, $C_{L\alpha}$ is assumed to be constant over the wingspan (Figure 3.4 – left panel). Bowles (2014) suggested using an elliptical lift distribution with a wing tip loading of zero (Figure 3.4 – right panel).

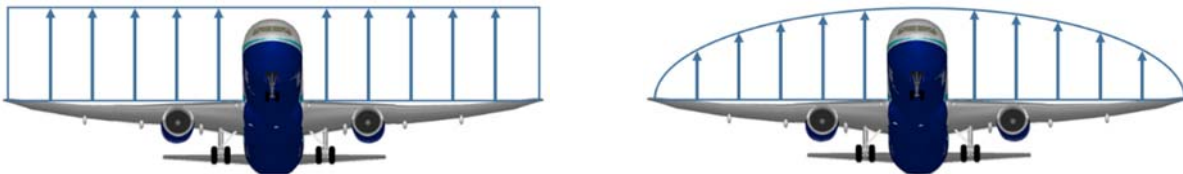


Figure 3.1. Constant and elliptical wing loading distributions (assuming rectangular wing in uniform flow).

The addition of elliptical loading term in Eq. (3.6) complicates the integral by introducing a square root term and requires numerical integration for its solution

$$C_{lv} = \frac{\Gamma_0 C_{L\alpha F} b_G}{\pi b_F^2 (1 + \lambda_F) V_F} \int_{-b_F/2b_G}^{b_F/2b_G} \left[\left(\bar{y} \left(1 - \frac{2b_G(1-\lambda_F)}{b_F} |\bar{y}| \right) \sqrt{1 - \left(\frac{2b_G \bar{y}}{b_F} \right)^2} \cdot \left[\frac{\bar{y} + (\bar{Y}_F + \bar{s}) \cos(\Phi) + \bar{Z}_F \sin(\Phi)}{\bar{y}^2 + \bar{y}(2(\bar{Y}_F + \bar{s}) \cos(\Phi) + 2\bar{Z}_F \sin(\Phi)) + ((\bar{Y}_F + \bar{s})^2 + \bar{Z}_F^2 + \bar{r}_c^2)} \right] - \left[\frac{\bar{y} + (\bar{Y}_F - \bar{s}) \cos(\Phi) + \bar{Z}_F \sin(\Phi)}{\bar{y}^2 + \bar{y}(2(\bar{Y}_F - \bar{s}) \cos(\Phi) + 2\bar{Z}_F \sin(\Phi)) + ((\bar{Y}_F - \bar{s})^2 + \bar{Z}_F^2 + \bar{r}_c^2)} \right] \right] d\bar{y} \quad (3.17)$$

Figures 3.5-3.7 show the comparison of C_{lv} calculation using Eq. 3.17 with the wind tunnel data for three different core radius sizes (2%, 4%, and 6% of the wingspan). Figures 3.8-3.10 show the comparison of the original method with the modified method for $r_c = 6\%$. There is a noticeable reduction in errors for Wings 1, and 5. However, the C_{lv} for Wing 4 is now underestimated for core radius size of 6%.

Results of the error analysis are given in Table 3.5. A Burnham-Hallock model was used to characterize the vortex flow field with the core radius size of 6% in these calculations.

Table 3.5: Modified Bowles-Tatnall Method

Wing	C_{lv}		
	rmse	mae	bias
1	0.0087	0.0054	0.0002
4	0.0140	0.0111	0.0030
5	0.0053	0.0041	0.0012

It is important to note that for both the original and the modified Bowles-Tatnall methods, the computed results are well within the uncertainty bounds of the wind tunnel measurements which are plotted in Tatnall (1995).

Once the rolling moment coefficient has been calculated for the initial circulation strength value, Γ_0 , from Eq. (3.17), the time history of C_{lv} can be estimated from the circulation decay history (Appendix B). In the current implementation, the time history of wake vortex circulation decay is obtained from the fast-time models. Several idealized vortex models have been proposed in the past besides the Burnham-Hallock model for characterizing the aircraft wake flowfield. The rolling moment coefficient calculations using these models are presented in Appendix C.

The C_{lv} estimates obtained from the Bowles-Tatnall method can be used to calculate maximum vortex-induced roll angle (Tatnall 1995, Appendix D). This calculation, however requires additional aircraft parameters which may not be readily available. These parameters include the pilot input roll control corresponding to maximum aileron deflection, the roll damping coefficient of the follower, and the roll moment of inertia of the follower, etc. A database of these parameters for a small set of different aircraft is given in Tatnall (1995).

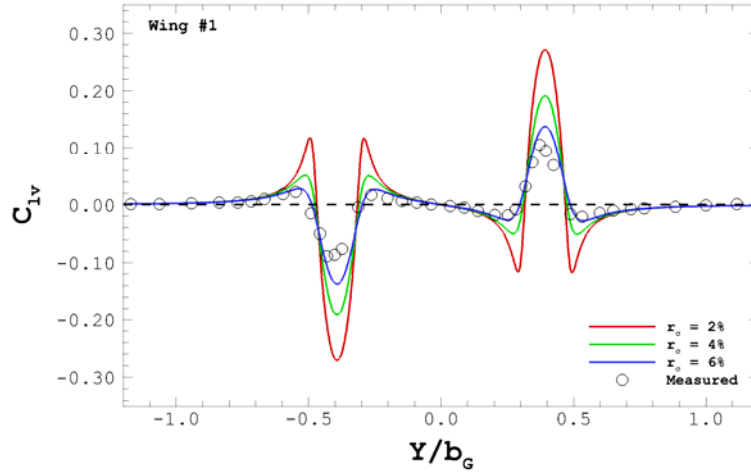


Figure 3.2. Comparison of measured and computed C_{lv} for varying r_c values for Wing #1.

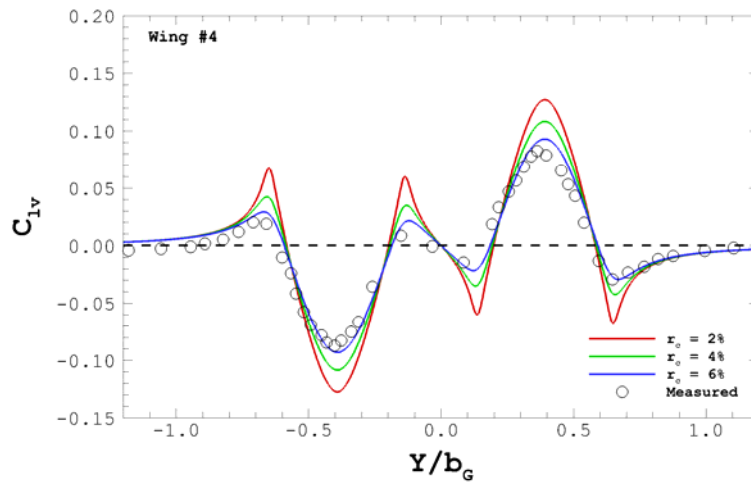


Figure 3.3. Comparison of measured and computed C_{lv} for varying r_c values for Wing #4.

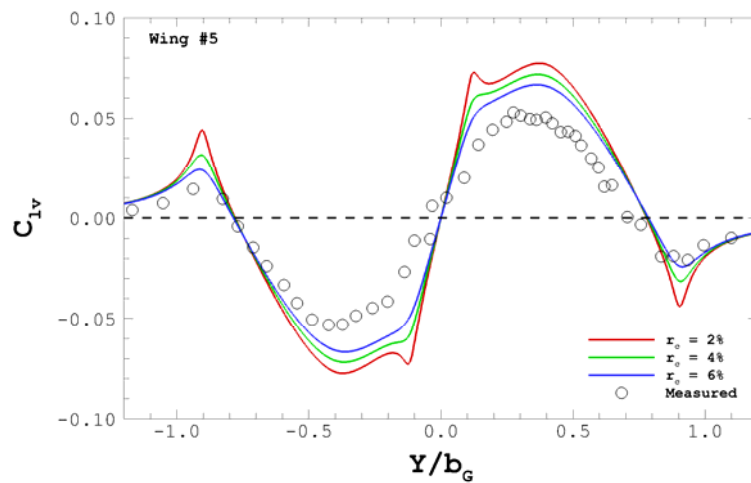


Figure 3.4. Comparison of measured and computed C_{lv} for varying r_c values for Wing #5.

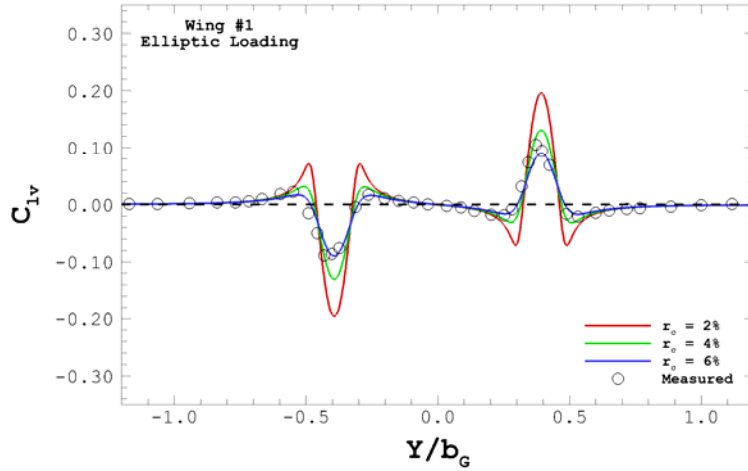


Figure 3.5. Comparison of measured and computed C_{lv} for varying r_c values for Wing #1.

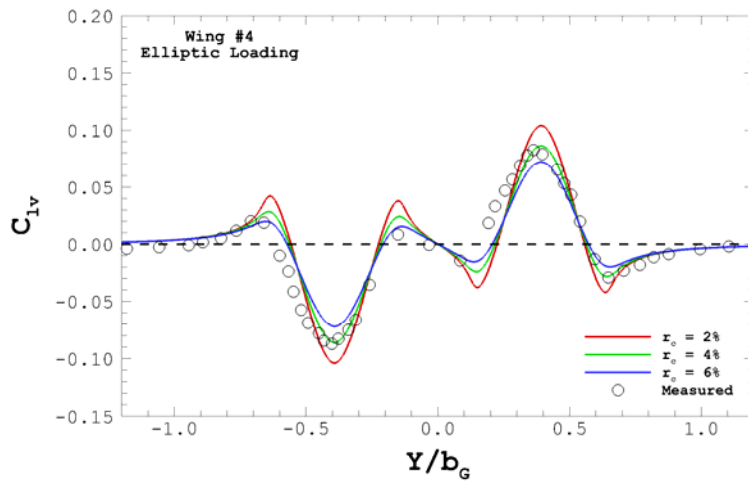


Figure 3.6. Comparison of measured and computed C_{lv} for varying r_c values for Wing #4.

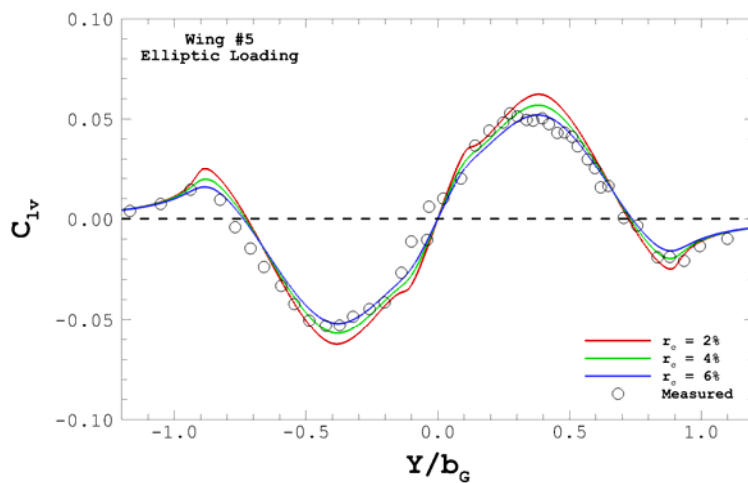


Figure 3.7. Comparison of measured and computed C_{lv} for varying r_c values for Wing #5.

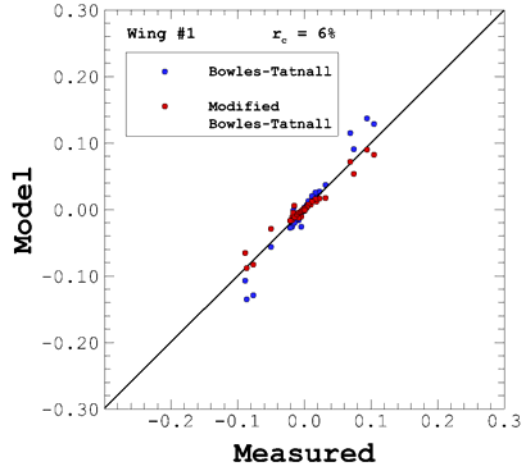


Figure 3.8. Wing #1: Comparison of modeled vs. measured vortex-induced rolling moment coefficient, C_{l_v} for core radius size of 6% of the wingspan.

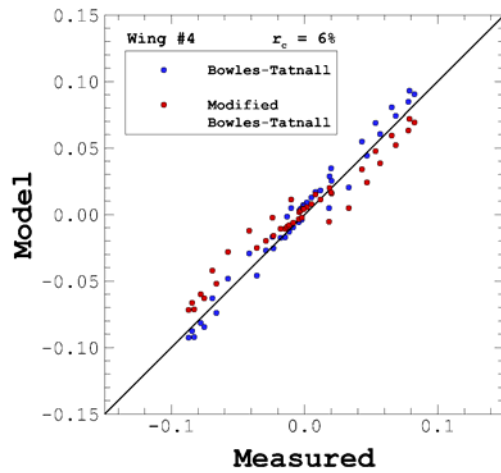


Figure 3.9. Wing #4: Comparison of modeled vs. measured vortex-induced rolling moment coefficient, C_{l_v} for core radius size of 6% of the wingspan.

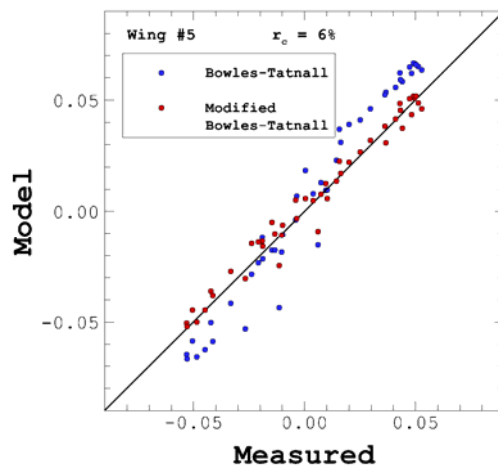


Figure 3.10. Wing #5: Comparison of modeled vs. measured vortex-induced rolling moment coefficient, C_{l_v} for core radius size of 6% of the wingspan.

4. Wake Encounter Analysis

A Cessna Citation 550 aircraft (N753CC) crashed at the Will Rogers World Airport (OKC) in Oklahoma City, Oklahoma on December 21, 2012. Neither the pilot nor the co-pilot were seriously injured. The crash could have been caused by the wake vortices of an Airbus A300-600 (heavy category aircraft), which had landed on the same runway about one minute prior to the crash. The National Transportation Safety Board (NTSB) carried out an investigation of this accident and concluded that the accident was likely due to an inadvertent wake encounter (O'Callaghan, 2013). To determine the likelihood of a wake vortex encounter, an analysis of the data used in the NTSB investigation is presented using the wake analysis tool described in earlier sections.

The input data for the analysis was obtained from the NTSB report and included aircraft trajectories, aircraft parameters, and weather data. The Cessna's trajectory and its initial point of impact is shown in Figure 4.1 (O'Callaghan, 2013). Figure 4.2 shows the Cessna's approach ten seconds, three seconds, and one second before the initial impact respectively. Publicly available data from the airport surveillance radar and the Cessna's onboard Enhanced Ground Proximity Warning System (EGPWS) provided both aircraft's latitude, longitude, altitude, the Cessna's orientation and airspeed.

The report also includes the National Weather Service's Meteorological Aerodrome Report and Automated Surface Observation System (ASOS) measurements which provided additional ground-level wind data from eight minutes before and one minute after the accident.



Figure 4.1. Google Earth overlay of Cessna flight path. Image from NTSB Accident CEN13TA113, Docket Item 11, EGPWS Factual Report. Times are in UTC.

The trajectory and the circulation strength of the wake vortices were simulated using the probabilistic wake vortex model described in Section 2. The simulated wake vortex bounds are shown in Figure 4.3. The red trajectory through the red crosses is the trajectory of the Airbus, while the blue trajectory indicates the Cessna's flight path. The red lines forming the enclosed boxes indicate the maximum bound within which the wake vortices could be present according to the simulation ($\pm 2\sigma$ -bounds). The colors of the boxes correspond to the vortex strength at those points, as indicated by the legend. The strength of the vortices predicted in this analysis corresponds well with the findings in the aircraft performance wake vortex study carried out by the NTSB. The general direction in which the vortices move is also consistent with the report. Because the current study uses $\pm 2\sigma$ -bounds based on the probabilistic wake vortex predictions the hazard

region denoted by the boxes in Figure 4.3 encloses a wider area compared to the deterministic trajectories shown in the NTSB report.

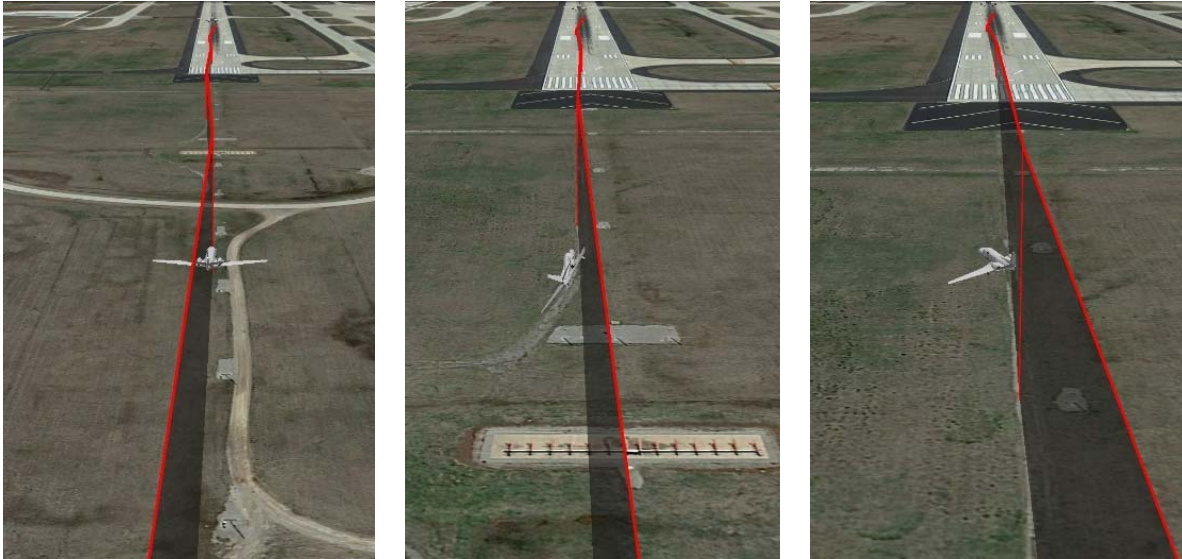


Figure 4.2. Position of the Cessna ten seconds (left panel); three seconds (middle panel); and one second before the ground impact (right panel). The Airbus trajectory is shown in red.

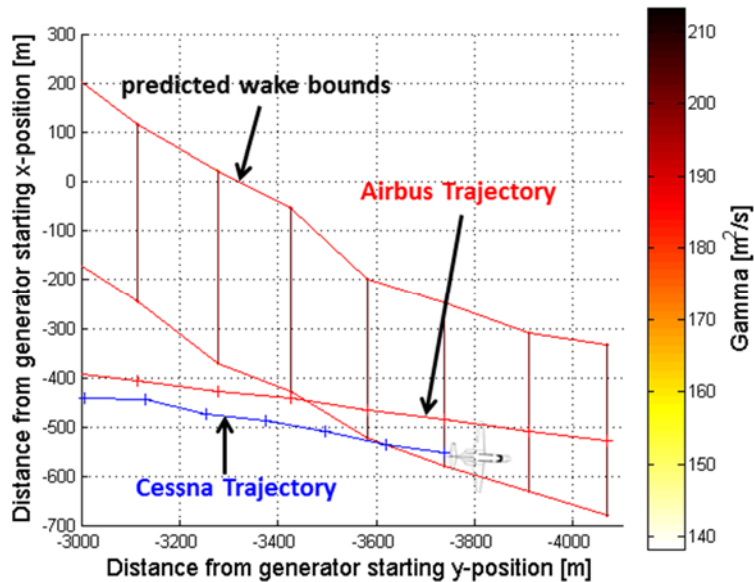


Figure 4.3. Wake vortex hazard bounds. The time window is approximately between 15:58:11 to 15:59:20UTC. The accident time was around 15:59:22UTC. The plot corresponds to Figure 13a (top right) in (O’Callaghan, 2013).

Figures 4.4-4.6 show the simulated wake vortex bounds being created, evolving, and drifting downwind, and encountering the Cessna moments before its unexpected roll. The red boxes indicate the maximum range where wake vortex centers are expected within the 2σ -bounds. This prediction qualitatively agrees with the NTSB report’s estimated vortex location which also indicates a probable vortex encounter immediately before the Cessna’s un-commanded roll.



Figure 4.4. A300 and its track is shown in the figure along with the APA predicted vortex bounds.



Figure 4.5. Transport of A300 wake by crosswinds predicted by the APA simulation.



Figure 4.6. Cessna encountering the wake bounds predicted by the APA simulation.

The circulation strength of the A300’s right wingtip vortex at the time of the potential encounter according was estimated by the probabilistic wake vortex model to be 2,319 ft²/s. This is consistent with the NTSB’s finding of circulation strengths up to approximately 2,300 ft²/s. The aircraft response was calculated using the Bowles-Tatnall method and the modified version using the elliptical wing loading as described in Section 3. Burnham-Hallock and Rankine vortex models were used in this calculation. The Rankine vortex model was used in the NTSB calculations. The results are given in Table 4.1. A C_{lv} value of approximately 0.152 was estimated using the modified Bowles-Tatnall method with Rankine vortex model. This corresponds to an induced roll of up to 153% of the maximum roll counter control provided by the Cessna’s ailerons.

Table 4.1: Estimates of Vortex-Induced Rolling Moment Coefficient

Method	C_{lv}	
	Burnam-Hallock	Rankine
Bowles-Tatnall	0.1617	0.1841
Modified Bowles-Tatnall	0.1306	0.152
O’Callaghan (2013)	NA	0.15

According to the NTSB’s Pilot/Operator Aircraft Accident/Incident Report the pilot and co-pilot “discussed wake turbulence avoidance procedures and planned to make a steeper approach and land beyond the Airbus’s touchdown point.” However, the Cessna’s trajectory according to the flight recorder data (Figure 4.2) shows the Cessna flying below the Airbus's glide path.

NTSB’s Aircraft Performance Wake Vortex Study concluded that, “Consequently, while it is impossible to establish conclusively that wake turbulence from the Airbus was responsible for the large left roll experienced by N753CC, the data relevant to the problem indicate that (1) N753CC very likely encountered the right wake vortex of the Airbus, and (2) this encounter very likely generated strong rolling moments to the left that can account for the 60° roll to the left recorded by the EGPWS on N753CC.” These conclusions are consistent with the results obtained in the current study.

5. Summary

A methodology for the development and integration of probabilistic wake vortex models with aircraft response model for air traffic management applications was presented. The two modules 1) probabilistic wake prediction, and 2) aircraft response to wake encounter, were evaluated independently using data from field experiments and wind tunnel tests with favorable results. The performance of the coupled probabilistic wake and aircraft response model was evaluated using data from an NTSB investigation. Figure 5.1 shows a schematic of the developed system.

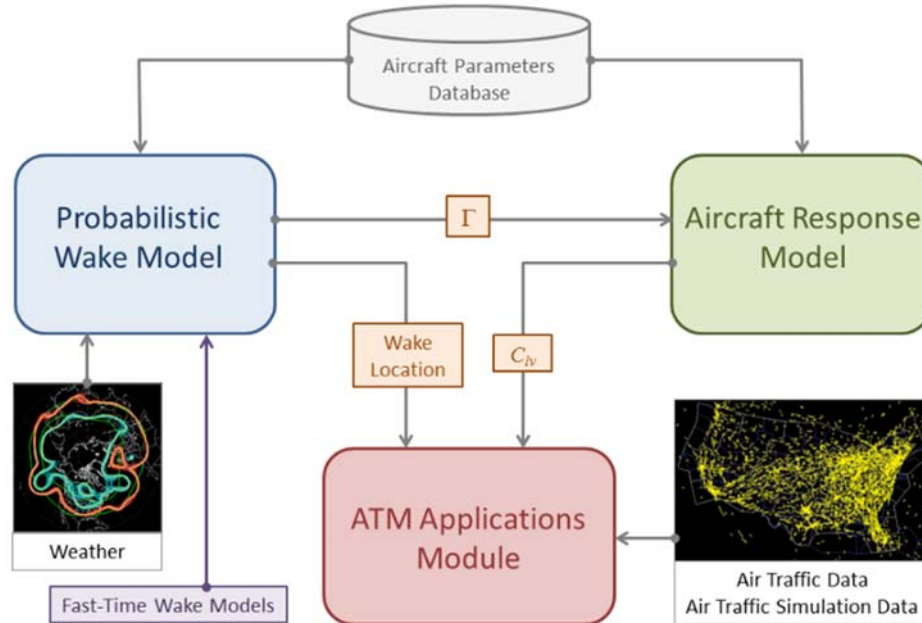


Figure 5.1. Integration of probabilistic wake prediction models with aircraft response models for ATM concepts development and safety analysis. The air traffic image in the figure shows the results of a simulation using NASA’s Future ATM Concepts Evaluation Tool (FACET) developed by Bilmoria et al. (2001).

The Monte-Carlo method described in this report is relatively simple to implement and integrate with the aircraft response models. It can effectively account for uncertainties in the atmospheric and aircraft-dependent initial conditions and provide an envelope of wake hazard region. The accuracy of Monte-Carlo simulations depends on reliable pdfs that represent the uncertainties in the initial conditions. In this study, the weather pdfs were built using the data collected during the two field campaigns. The pdfs can also be generated using other methods,

- means estimated by onboard sensors and pdfs constructed from climatological data
- instrument uncertainty can be used (if available) for defining pdfs
- mean profiles from mesoscale numerical weather prediction (NWP) models and pdfs constructed from climatological data

The methodology as described in this report is well-suited for systems-level design and safety analysis of new advanced ATM concepts as well as forensic reconstruction of accidents due to inadvertent wake encounters. However, for use as a real-time dynamic spacing tool (airborne or ground-based) more research is needed for the definition of weather pdfs. Current results showed that the lateral location of the vortex pair was well bounded compared to the vertical location and the circulation strength. The results also showed that a multi model ensemble approach can improve the solution. Further improvements might be possible by generating non-constant weather perturbation profiles.

The Bowles-Tatnall method and its modified versions were evaluated using wind tunnel data and integrated with the fast-time probabilistic model. Evaluations with wind tunnel data showed that the method is accurate and reliable – the differences in the model predictions and wind tunnel measurements were low and well within the bounds of measurement uncertainty. A sensitivity study was conducted to see the effect of different vortex models and vortex core radius size on the accuracy of the method. The modified Bowles-Tatnall method using either the Burnham-Hallock or the Proctor vortex model with a core radius size set to 6% of the wing span gave the best results. The calculation of rolling moment coefficient in the current implementation requires the following inputs:

- wake circulation strength (obtained from the probabilistic wake model)
- generator parameters: wingspan, and the vortex pair separation
- follower parameters: wingspan, airspeed, wing taper ratio, and the lift-curve slope

Much work to date in the application of wake vortex research has been toward redefining the standard separation distances and times between aircraft of various weight categories for take-off, landing, and en route operations. While these efforts have been successful in further refining these standards, the development of fast and accurate models for the prediction of wake vortex hazards in real time holds promise for more flexible applications in air traffic management.

When considering wake vortex constraints in air traffic operations, the fundamental tradeoff is between safety and capacity in driving the standard separation distances between aircraft. The driver of safety motivates larger, more conservative buffers between aircraft both en route and in the terminal area. This is directly opposed to the driver of capacity which requires smaller buffers in order to accommodate greater numbers of aircraft in a given airspace or at the runway threshold. The availability of a fast and accurate system to predict the wake vortex interaction between any pair of aircraft in real time can allow the dynamically optimized minimum separation standard between those aircraft, thus increasing capacity without compromising safety.

While such a tool has obvious applications to the air traffic control paradigm of today, it is also potentially enabling for a class of new airborne ATM concepts. Consider a concept for airborne self-separation such as the Autonomous Flight Rules (Wing and Cotton 2011). In this concept, the aircrew on the flight deck assume responsibility for separation, enabled by an onboard automation system for detecting and resolving air traffic conflicts using onboard surveillance systems such as ADS-B. The automation system acts as a replacement to the functions normally provided by air traffic controllers on the ground, and thus it should have awareness of operational hazards such as wake turbulence. A fast-time modeling approach such as the one developed in this report could be integrated into the automation system for predicting the vortex trajectory and aircraft response and providing a dynamically-optimized keep-out region for the pilot to avoid. The prediction is made accurate by the use of aircraft parameters and local meteorological measurements shared between aircraft in the vicinity over air-to-air communications as well as through a System-Wide Information Management (SWIM) uplink from the ground. A dynamically-defined, wake-aware separation management has similar applications to Interval Management (Barmore et al. 2014) and numerous other concepts of operation.

In addition to the operational applications, the approach developed here also has applications to the safety analysis of ATM concepts during the design phase. By incorporating the coupled probabilistic wake and aircraft response model into fast-time air traffic simulations, the frequency and severity of wake vortex encounters can be evaluated for a given operational concept. The wake hazard can be understood and mitigated early in the design phases of the concept rather than in later stages of development where conceptual changes are much more costly.

Acknowledgment

The support and encouragement of Lisa Rippy, Steve Velotas, and Neil O'Connor throughout this effort is gratefully acknowledged.

Appendix A: Derivation of Rolling Moment Coefficient

The derivation of the Bowles-Tatnall method (Tatnall 1995) is reproduced here for the sake of completeness. The method is based on the aerodynamic strip theory (von Mises 1959). The flowfield generated by the wake vortices is modeled using the Burnham-Hallock vortex model. The vortices, shed by the generating aircraft, are assumed to be two-dimensional in the wake far-field. The tangential velocity, W_T , of a single vortex based on the Burnham-Hallock vortex model is given by

$$W_T = \frac{\Gamma(t)}{2\pi r \left(1 + \left(\frac{r_c}{r} \right)^2 \right)}, \quad (\text{A.1})$$

where, $\Gamma(t)$ is the total farfield vortex circulation at time t , r is the radial distance from the two-dimensional vortex center, and r_c is the vortex-core radius. The two vortices are superimposed to obtain the vortex pair. The axis conventions used in this appendix follow Tatnall (1995) and are shown in Figure A.1.

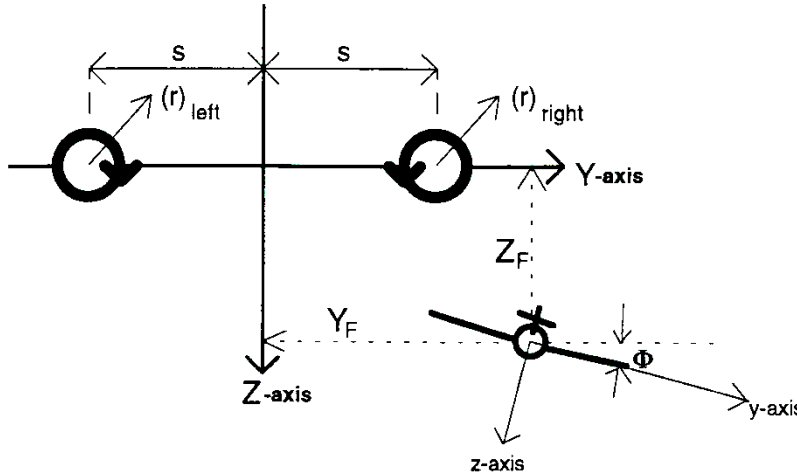


Figure A.1. Axis conventions used in the derivation of the rolling moment coefficient (Tatnall 1995).

The tangential velocity can be expressed in Cartesian coordinates by substituting $\sqrt{(Y+s)^2 + Z^2}$ and $\sqrt{(Y-s)^2 + Z^2}$ for r in Eq. (A.1) for the left and right vortices respectively

$$(W_T)_{left} = \frac{\Gamma(t)}{2\pi \left(\sqrt{(Y+s)^2 + Z^2} \right) \left(1 + \frac{r_c^2}{\left(\sqrt{(Y+s)^2 + Z^2} \right)^2} \right)}, \quad (\text{A.2})$$

$$(W_T)_{right} = \frac{\Gamma(t)}{2\pi \left(\sqrt{(Y-s)^2 + Z^2} \right) \left(1 + \frac{r_c^2}{\left(\sqrt{(Y-s)^2 + Z^2} \right)^2} \right)}. \quad (\text{A.3})$$

An elliptical lift distribution is assumed for the generating aircraft; therefore, s is defined as

$$s = b_G \left(\frac{\pi}{8} \right). \quad (\text{A.4})$$

The sum of the components of Eq. (A.3) and (A.4) gives the complete flow field. The left and right vortices have the same magnitude and opposite circulation,

$$W_Y = -(W_T)_{left} \left(\frac{Z}{\sqrt{(Y+s)^2 + Z^2}} \right) + (W_T)_{right} \left(\frac{Z}{\sqrt{(Y-s)^2 + Z^2}} \right), \quad (\text{A.5})$$

$$W_Z = (W_T)_{left} \left(\frac{Y+s}{\sqrt{(Y+s)^2 + Z^2}} \right) - (W_T)_{right} \left(\frac{Y-s}{\sqrt{(Y-s)^2 + Z^2}} \right). \quad (\text{A.6})$$

Re-writing Eq. (A.6) and (A.7) in terms of vortex circulation strength

$$W_Y = -\frac{\Gamma(t)Z}{2\pi((Y+s)^2 + Z^2 + r_c^2)} + \frac{\Gamma(t)Z}{2\pi((Y-s)^2 + Z^2 + r_c^2)}, \quad (\text{A.7})$$

$$W_Z = \frac{\Gamma(t)(Y+s)}{2\pi((Y+s)^2 + Z^2 + r_c^2)} - \frac{\Gamma(t)(Y-s)}{2\pi((Y-s)^2 + Z^2 + r_c^2)}. \quad (\text{A.8})$$

The inertial-axis velocity components in Eq. (A.8) and (A.9) can be transformed into induced velocity components, w_{b_y} , and w_{b_z} in the body-axis system using the inverse transformation,

$$\begin{bmatrix} w_{b_y} \\ w_{b_z} \end{bmatrix} = \begin{bmatrix} \cos(\Phi) & \sin(\Phi) \\ -\sin(\Phi) & \cos(\Phi) \end{bmatrix} \begin{bmatrix} W_Y \\ W_Z \end{bmatrix} = \begin{bmatrix} W_Y \cos(\Phi) + W_Z \sin(\Phi) \\ -W_Y \sin(\Phi) + W_Z \cos(\Phi) \end{bmatrix}, \quad (\text{A.9})$$

and the transformation,

$$\begin{bmatrix} Y \\ Z \end{bmatrix} = \begin{bmatrix} Y_F \\ Z_F \end{bmatrix} + \begin{bmatrix} \cos(\Phi) & -\sin(\Phi) \\ \sin(\Phi) & \cos(\Phi) \end{bmatrix} \begin{bmatrix} y \\ z \end{bmatrix} = \begin{bmatrix} Y_F + y \cos(\Phi) - z \sin(\Phi) \\ Z_F + y \sin(\Phi) + z \cos(\Phi) \end{bmatrix}, \quad (\text{A.10})$$

where, (Y, Z) is the location in the inertial axis system, (y, z) is the location in the body-axis system, and the location of the aircraft's center of gravity in inertial coordinates is denoted by (Y_F, Z_F) .

The induced angle of attack can be obtained from the small angle approximation,

$$\alpha_i = \arctan \left(-\frac{w_{b_z}}{V_F} \right) \cong -\frac{w_{b_z}}{V_F}, \quad (\text{A.11})$$

In Eq. (A.12) V_F is the following aircraft's airspeed. Using Eq. (A.8), (A.9), (A.10), and (A.11) for w_{b_z} into (A.12),

$$\alpha_i = -\frac{\Gamma(t)}{2\pi V_F} \bullet \left\{ \left[\frac{y + ((Y_F + s)\cos(\Phi) + Z_F \sin(\Phi))}{y^2 + (2(Y_F + s)\cos(\Phi) + 2Z_F \sin(\Phi))y + ((Y_F + s)^2 + Z_F^2 + r_c^2)} \right] \right. \\ \left. - \left[\frac{y + ((Y_F - s)\cos(\Phi) + Z_F \sin(\Phi))}{y^2 + (2(Y_F - s)\cos(\Phi) + 2Z_F \sin(\Phi))y + ((Y_F - s)^2 + Z_F^2 + r_c^2)} \right] \right\}. \quad (\text{A.12})$$

Normalizing all lengths in Eq. (A.12) by the generator wingspan, which is indicated with a bar above each symbol,

$$\alpha_i = -\frac{\Gamma(t)}{2\pi V_F b_G} \bullet \left\{ \left[\frac{\bar{y} + ((\bar{Y}_F + \bar{s})\cos(\Phi) + \bar{Z}_F \sin(\Phi))}{\bar{y}^2 + (2(\bar{Y}_F + \bar{s})\cos(\Phi) + 2\bar{Z}_F \sin(\Phi))\bar{y} + ((\bar{Y}_F + \bar{s})^2 + \bar{Z}_F^2 + \bar{r}_c^2)} \right] \right. \\ \left. - \left[\frac{\bar{y} + ((\bar{Y}_F - \bar{s})\cos(\Phi) + \bar{Z}_F \sin(\Phi))}{\bar{y}^2 + (2(\bar{Y}_F - \bar{s})\cos(\Phi) + 2\bar{Z}_F \sin(\Phi))\bar{y} + ((\bar{Y}_F - \bar{s})^2 + \bar{Z}_F^2 + \bar{r}_c^2)} \right] \right\}. \quad (\text{A.13})$$

The roll-moment coefficient, C_{l_v} can be determined from the induced angle of attack by employing strip theory. The follower's wing is modeled as a flat, and linearly-tapered wing. The modeled wing is divided into small elements along the wingspan, and the rolling moment contribution is determined for each element. It is assumed that each element experiences a uniform flow independent from the other elements. The result for the complete wing can be obtained by finding the total contribution of all wing elements (integration over the wingspan)

$$C_{l_v}(Y_F, Z_F, \Phi) = \frac{l_v(Y_F, Z_F, \Phi)}{\bar{q} S_F b_F} \cong \frac{- \int_{-b_F/2}^{b_F/2} C_{L_{\alpha F}} \cdot \alpha_i(y, Y_F, Z_F, \Phi) \cdot c_F(y) \cdot \bar{q} \cdot y \cdot dy}{\bar{q} S_F b_F}, \quad (\text{A.14})$$

l_v , S_F , b_F , $C_{L_{\alpha F}}$, and $c_F(y)$ are the follower's: roll, planform area, wingspan, three-dimensional wing lift-curve slope, and the local wing chord respectively. \bar{q} is the freestream dynamic pressure. For most aircraft, the local chord can be approximated from a linearly-tapered planform using

$$c_F(y) = \frac{2S_F}{b_F(1 + \lambda_F)} \left(1 - \frac{2(1 - \lambda_F)}{b_F} |y| \right), \quad (\text{A.15})$$

where λ_F is the follower's wing taper ratio. Eq. (A.14) and (A.16) can be substituted into (A.15) using normalization with b_G in order to obtain the expression for the vortex-induced rolling moment coefficient,

$$C_{l_v} = \frac{\Gamma(t) C_{L_{\alpha F}} b_G}{\pi b_F^2 (1 + \lambda_F) V_F} \int_{-b_F/2}^{b_F/2} \left\{ \bar{y} \left(1 - \frac{2b_G(1 - \lambda_F)}{b_F} |\bar{y}| \right) \bullet \left[\frac{\bar{y} + ((\bar{Y}_F + \bar{s})\cos(\Phi) + \bar{Z}_F \sin(\Phi))}{\bar{y}^2 + \bar{y}(2(\bar{Y}_F + \bar{s})\cos(\Phi) + 2\bar{Z}_F \sin(\Phi)) + ((\bar{Y}_F + \bar{s})^2 + \bar{Z}_F^2 + \bar{r}_c^2)} \right] \right. \\ \left. - \left[\frac{\bar{y} + ((\bar{Y}_F - \bar{s})\cos(\Phi) + \bar{Z}_F \sin(\Phi))}{\bar{y}^2 + \bar{y}(2(\bar{Y}_F - \bar{s})\cos(\Phi) + 2\bar{Z}_F \sin(\Phi)) + ((\bar{Y}_F - \bar{s})^2 + \bar{Z}_F^2 + \bar{r}_c^2)} \right] \right\} d\bar{y} \quad (\text{A.16})$$

Eq. (A.16) can be solved analytically and the solution is provided in Tatnall (1995) and in Section 3 of this document.

Appendix B: Calculation of C_{Iv} at Time t

The vortex-induced rolling moment coefficient as a function of time is related to the circulation strength decay by the following relation (Tatnall 1995):

$$C_{Iv}(t) = \frac{\Gamma(t)}{\Gamma(0)} C_{Iv}(0), \quad (\text{B.1})$$

where, $C_{Iv}(0)$ is the vortex-induced rolling moment coefficient due to initial vortex circulation strength $\Gamma(0) = \Gamma_0$. Given the circulation decay time history from the fast-time wake models, the evolution of rolling moment coefficient in time can be estimated.

Appendix C: Sensitivity to Vortex Model

The Bowles-Tatnall method as described in Tatnall (1995) uses the Burnham-Hallock vortex model for defining the vortex flow field. A sensitivity analysis was performed to evaluate the performance of the method using other idealized vortex models (Gerz et al. 2002; Ahmad et al. 2014a).

Idealized Vortex Models

Lamb-Oseen Model

The Lamb-Oseen vortex is an analytical solution of the Navier-Stokes equations (Ahmad et al. 2014a). The tangential velocity, v_θ as a function of radial distance, r from the vortex center in the Lamb-Oseen model is given by (Holzäpfel et al. 2000)

$$v_\theta(r) = \frac{\Gamma_0}{2\pi r} \left[1 - \exp\left(-1.26(r/r_c)^2\right) \right], \quad (\text{C.1})$$

where r_c is the vortex core radius, Γ_0 is the vortex circulation, and r is the distance from vortex center (y_0, z_0)

$$r = \sqrt{(y - y_0)^2 + (z - z_0)^2}. \quad (\text{C.2})$$

Burnham-Hallock Model

The Burnham-Hallock model (Burnham and Hallock 1982) is given by Eq. (C.3). It is the most widely used model for wake vortex applications.

$$v_\theta(r) = \frac{\Gamma_0}{2\pi r} \frac{r^2}{r^2 + r_c^2}. \quad (\text{C.3})$$

Proctor Model

The Proctor vortex model (Proctor et al. 2000) is based on lidar observations of the vortex tangential velocity, and is given by

$$v_\theta(r) = \begin{cases} 1.0939 \frac{\Gamma_0}{2\pi r} \left[1 - \exp\left(-10(1.4r_c/b_G)^{0.75}\right) \right] \times \left[1 - \exp\left(-1.2527(r/r_c)^2\right) \right] & \text{if } r \leq 1.4r_c \\ \frac{\Gamma_0}{2\pi r} \left[1 - \exp\left(-10(r/b_G)^{0.75}\right) \right] & \text{if } r > 1.4r_c \end{cases}, \quad (\text{C.4})$$

where b_G is the wingspan of the wake generator.

Rankine Model

The tangential velocity of the Rankine vortex model (Gerz et al. 2002) is given by

$$v_{\theta}(r) = \begin{cases} \frac{\Gamma_0}{2\pi r_c} \frac{r}{r_c} & \text{if } r \leq r_c \\ \frac{\Gamma_0}{2\pi r} & \text{if } r > r_c \end{cases} . \quad (\text{C.5})$$

Winckelmans Model

The Winckelmans model (Gerz et al. 2002) is given by

$$v_{\theta}(r) = \frac{\Gamma_0}{2\pi r} \left\{ 1 - \exp \left[- \frac{\beta_i (r/b)^2}{\left[1 + \{ (\beta_i / \beta_o) (r/b)^{5/4} \}^p \right]^{1/p}} \right] \right\}, \quad (\text{C.6})$$

where $\beta_o = 10$, $\beta_i = 500$, and $p = 3$.

Jacquin Model

The Jacquin vortex model (Gerz et al. 2002) is given by

$$v_{\theta}(r) = \begin{cases} \frac{\Gamma_0}{2\pi r_i} \frac{r}{(r_i r_o)^{1/2}} & \text{for } r \leq r_i \\ \frac{\Gamma_0}{2\pi (r_o r)^{1/2}} & \text{for } r_i \leq r \leq r_o, \\ \frac{\Gamma_0}{2\pi r} & \text{for } r \geq r_o \end{cases} \quad (\text{C.7})$$

where $r_i \leq 0.01b_G$ and $r_o \approx 0.1b_G$.

Sensitivity Analysis

The modified Bowles-Tatnall method was used in the sensitivity analysis. The vortex core radius size was set to $0.06b_G$. The root mean square errors based on the wind tunnel data are given in Table C.1 and the results are plotted in Figures C1-C3 for the three different wings. In general, the Burnham-Hallock vortex model tends to result in lower values for the rolling moment coefficient and the Rankine model gives the highest values. The Burnham-Hallock model gave the least error for Wing 1 and Wing 5, and the Proctor model had the least error for Wing 4.

Table C.1: Modified Bowles-Tatnall Method – $r_c = 6\%$

Vortex Model	C_{lv}		
	Wing #1	Wing #4	Wing #5
BH	0.0087	0.0140	0.0053
LO	0.0132	0.0131	0.0067
FP	0.0092	0.0129	0.0056
Wi	0.0142	0.0130	0.0059
Ja	0.0322	0.0155	0.0079
Ra	0.0187	0.0141	0.0073

BH = Burnham-Hallock; LO = Lamb-Oseen; FP = Proctor; Wi = Winckelmans; Ja = Jacquin; Ra = Rankine

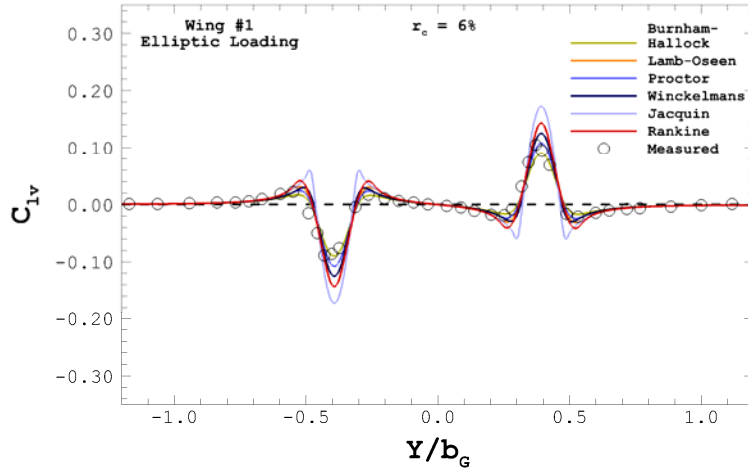


Figure C.1. Measured and computed C_{lv} using different vortex models for Wing #1.

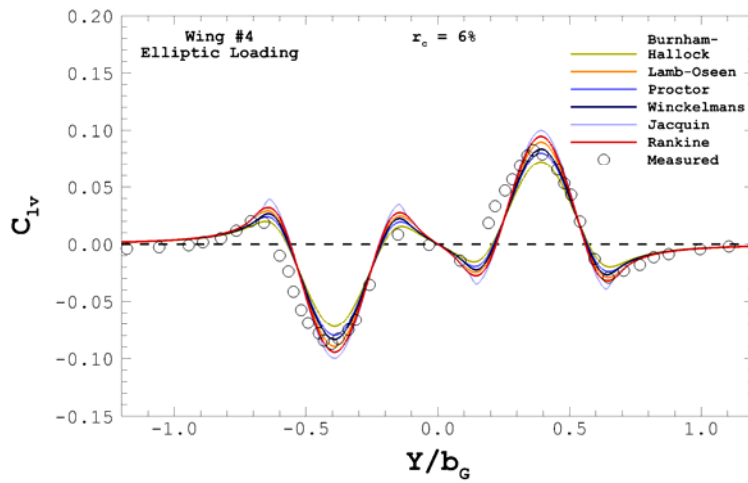


Figure C.2. Measured and computed C_{lv} using different vortex models for Wing #4.

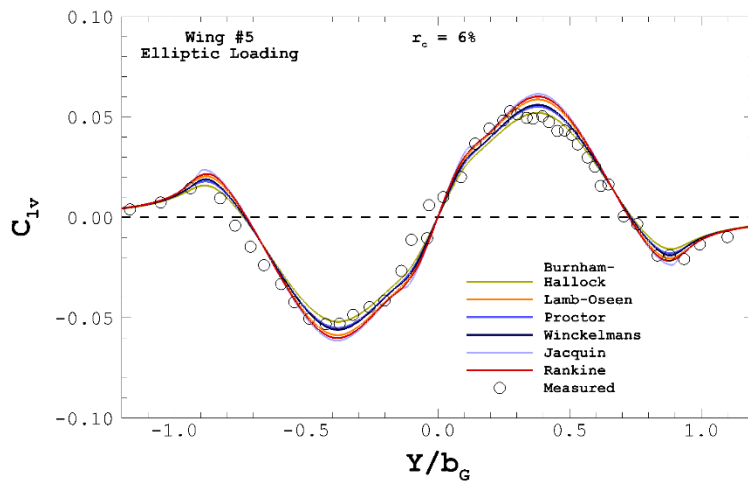


Figure C.3. Measured and computed C_{lv} using different vortex models for Wing #5.

Appendix D: Maximum Vortex-Induced Roll Angle

The vortex-induced maximum roll angle can be approximated using a one degree-of-freedom (1DoF) model (Tatnall 1995)

$$\phi_{\max} = \phi_{\infty} \left[1 + \frac{R(T_c - T_m)}{T_v} \right], \quad (\text{D.1})$$

where, $\phi_{\infty} = -\frac{K_1 C_{l_v} T_v}{K_2}$, is the maximum bank angle of the aircraft without control input. The dynamic pressure q , and, the parameters, K_1 , K_2 and, R are given by

$$K_1 = \frac{q S_F b_F}{I_{xx}}; \quad K_2 = \frac{K_1 C_{l_{\bar{p}}} b_F}{2V_F}; \quad R = \frac{C_{l_c}}{C_{l_v}}; \quad q = \frac{\rho V_F^2}{2}. \quad (\text{D.2})$$

The time at which the bank angle reaches a maximum is given by

$$T_m = -\frac{1}{K_2} \ln \left(\frac{R e^{-K_2 T_c} + e^{-K_2 T_v} - 1}{R} \right). \quad (\text{D.3})$$

In Eq. (D.2), $C_{l_c} = 0.07 |C_{l_{\bar{p}}}|$ is the pilot input roll control corresponding to maximum aileron deflection, and $C_{l_{\bar{p}}}$ is the roll damping coefficient of the follower. T_c is the time of control input activation and, T_v is the time of vortex impulse deactivation, and I_{xx} is the roll moment of inertia.

References

Ahmad, NN, FH Proctor, “Estimation of Eddy Dissipation Rates from Mesoscale Model Simulations”, American Institute of Aeronautics and Astronautics, AIAA Paper 2012-0429.

Ahmad, NN, FH Proctor, RL VanValkenburg, MJ Pruis, FM Limon Duparcmeur, “Mesoscale Simulation Data for Initializing Fast-Time Wake Transport and Decay Models”, American Institute of Aeronautics and Astronautics, AIAA Paper 2013-0510. 2013a.

Ahmad, NN, FH Proctor, RB Perry, “Numerical Simulation of the Aircraft Wake Vortex Flowfield”, American Institute of Aeronautics and Astronautics, AIAA Paper 2013-2552. 2013b.

Ahmad, NN, FH Proctor, FM Limon Duparcmeur, D Jacob, “Review of Idealized Aircraft Wake Vortex Models”, American Institute of Aeronautics and Astronautics, AIAA Paper 2014-0927. 2014a.

Ahmad, NN, RL VanValkenburg, MJ Pruis, “NASA AVOSS Fast-Time Wake Prediction Models: User’s Guide,” National Aeronautics and Space Administration, 2014, NASA/TM-2014-218152. 2014b.

Ahmad, NN, RL VanValkenburg, RL Bowles, FM Limon Duparcmeur, T Gloudemans, S van Lochem, E Ras, “Evaluation of Fast-Time Wake Vortex Models using Wake Encounter Flight Test Data”, American Institute of Aeronautics and Astronautics, AIAA Paper 2014-2466. 2014c.

Ahmad, NN, MJ Pruis, "Evaluation of Fast-Time Wake Models using Denver 2006 Field Experiment Data," American Institute of Aeronautics and Astronautics, AIAA Paper 2015-3318.

Barmore, BE, NN Ahmad, MC Underwood, "Advanced Interval Management (IM) Concepts of Operations," National Aeronautics and Space Administration, 2014, NASA/TM-2014-218664.

Bilimoria, K, B Sridhar, G Chatterji, KS Seth, S Grabbe, "FACET: Future ATM concepts evaluation tool", *Air Traffic Control Quarterly* Vol. 9, 2001, pp. 1-20.

Bowles, DR, Personal communication. 2014.

Burnham, DC, JN Hallock, "Chicago Monostatic Acoustic Vortex Sensing System", U.S. Department of Transportation, DOT-TSC-FAA-79-103, 1982, 206 pp.

Burnham, DC, JN Hallock, "Decay Characteristics of Wake Vortices from Jet Transport Aircraft," *Journal of Aircraft*, Vol. 50, 2013, pp. 82-87.

Campbell, SD, et al., "Wake Vortex Field Measurement Program at Memphis, TN Data Guide", Lincoln Laboratory, Massachusetts Institute of Technology. Project Report NASA/L-2. 1997.

Corjon, A, T Poinot, "Vortex Model to Define Safe Aircraft Separation Distances," *Journal of Aircraft*, Vol. 33, 1996, pp. 547-553.

Delisi, DP, GC Greene, RE Robins, DC Vicroy, FY Wang, "Aircraft Wake Vortex Core Size Measurements", American Institute of Aeronautics and Astronautics, AIAA Paper 2003-3811.

De Visscher, I, G Winckelmans, T Lonfils, L Bricteux, M Duponcheel, N Bourgeois, "The Wake4D simulation platform for predicting aircraft wake vortex transport and decay: Description and examples of application", American Institute of Aeronautics and Astronautics, AIAA Paper 2010-7994.

Federal Aviation Administration, "Aircraft Wake Turbulence," Advisory Circular AC 90-23G. Effective Date: February 10, 2014.

Federal Aviation Administration, "Wake Turbulence Recategorization," FAA Order JO 7110.659C. Effective Date: February 29, 2016.

Feigh, KM, L Sankar, V Manivannan, "Statistical Determination of Vertical Resolution Requirements for Real-Time Wake-Vortex Prediction", *Journal of Aircraft*, Vol. 49, 2012, pp. 822-835.

Frech, M, F Holzäpfel, A Tafferner, T Gerz, "High-Resolution Weather Database for the Terminal Area of Frankfurt Airport", *Journal of Applied Meteorology and Climatology*, Vol. 46, 2007, pp. 1913-1932.

Frech, M, F Holzäpfel, "Skill of an aircraft wake-vortex model using weather prediction and observation," *Journal of Aircraft*, Vol. 45, 2008, pp. 461-470.

Gerz, T, F Holzäpfel, D Darracq, "Commercial aircraft wake vortices", *Progress in Aerospace Sciences*, Vol. 38, 2002, pp. 181-208.

Gerz, T, F Holzäpfel, W Gerling, A Scharnweber, M Frech, K Kober, K Dengler, S Rahm, "The Wake Vortex Prediction and Monitoring System WSVBS Part II: Performance and ATC Integration at Frankfurt Airport", *Air Traffic Control Quarterly* Vol. 17, 2009, pp. 323-346.

Green, GC, "An Approximate Model of Vortex Decay in the Atmosphere", *Journal of Aircraft*, Vol. 23, 1986, pp. 566-573.

Guerreiro, NM, KW Neitzke, SC Johnson, HP Stough, BT McKissick, HI Syed, "Characterizing a Wake-free Safe Zone for the Simplified Aircraft-based Paired Approach Concept", American Institute of Aeronautics and Astronautics, AIAA Paper 2010-7681.

Hallock, JN, GC Greene, JA Tittsworth, PD Strande, FY Wang, "Use of Simple Models to Determine Wake Vortex Categories for New Aircraft", American Institute of Aeronautics and Astronautics, AIAA Paper 2015-3172.

Han, J, SP Arya, S Shen, Y Lin, "An Estimation of Turbulent Kinetic Energy and Energy Dissipation Rate Based on Atmospheric Boundary Layer Similarity Theory", National Aeronautics and Space Administration, 2000, NASA/CR-2000-210298.

Han J, Y Lin, SP Arya, FH Proctor, "Numerical Study of Wake Vortex Decay and Descent in Homogeneous Atmospheric Turbulence," *AIAA Journal*, Vol. 38, 2000, pp. 643-656.

Hinton, DA, "Aircraft Vortex Spacing System (AVOSS) Conceptual Design", National Aeronautics and Space Administration, 1995, NASA/TM-1995-110184.

Hinton, DA, "An Aircraft Vortex Spacing System (AVOSS) For Dynamical Wake Vortex Spacing Criteria", Advisory Group for Aerospace Research and Development, North Atlantic Treaty Organization (NATO) , 1996, AGARD-CP-584.

Holzäpfel, F., T. Gerz, M. Frech, A. Dörnbrack, "Wake Vortices in Convective Boundary Layer and their Influence on Following Aircraft," *Journal of Aircraft*, Vol. 37, 2000, pp. 1001-1007.

Holzäpfel, F, "Probabilistic Two-Phase Wake-Vortex Decay and Transport Model," *Journal of Aircraft*, Vol. 40, 2003, pp. 323-331.

Holzäpfel, F, M Steen, "Aircraft wake-vortex evolution in ground proximity: Analysis and parameterization." *AIAA Journal*, Vol. 45, 2007, pp. 218-227.

Holzäpfel, F, M Frech, T Gerz, A Taffermer, K Hahn, C Schwarz, H Joos, B Korn, H Lenz, R Luckner, G Höhne, "Aircraft wake vortex scenarios simulation package - WakeScene", *Aerospace Science and Technology*, Vol. 13, 2009, pp. 1-11.

Holzäpfel, F, T Gerz, M Frech, A Taffermer, F Köpp, I Smalikho, S Rahm, K Hahn, C Schwarz, "The Wake Vortex Prediction and Monitoring System WSVBS Part I: Design". *Air Traffic Control Quarterly*, Vol. 17, 2009, pp. 302-322.

Holzäpfel, F, T Gerz, C Schwarz, "The Wake Vortex Prediction and Monitoring System WSVBS, Design and Performance at Frankfurt and Munich Airport", *Proceedings of the 9th USA/Europe Air Traffic Management Research and Development Seminar (ATM2011)*, 2011.

Holzäpfel, F, "Effects of Environmental and Aircraft Parameters on Wake Vortex Behavior", *Journal of Aircraft*, Vol. 51, 2014, pp. 1490-1500.

Johnson, SC, GW Lohr, BT McKissick, TS Abbott, NM Guerreiro, P Volk, "Simplified Aircraft-Based Paired Approach: Concept Definition and Initial Analysis", National Aeronautics and Space Administration, 2013, NASA/TP-2013-217994.

Körner, S, NN Ahmad, F Holzäpfel, RL VanValkenberg, "Multi-Model Ensemble Wake Vortex Prediction", American Institute of Aeronautics and Astronautics, AIAA Paper 2015-3173.

Lang, S, J Tittsworth, W Bryant, P Wilson, C Lepadatu, D Delisi, D Lai, G Greene, "Progress on an ICAO Wake Turbulence Re-Categorization Effort", American Institute of Aeronautics and Astronautics, AIAA Paper 2010-7682.

O'Callaghan, J, "Aircraft Performance Wake Vortex Study", National Transportation Safety Board, NTSB ID: CEN13TA113, 2013.

O'Connor, CJ, DK Rutishauser, "Enhanced Airport Capacity Through Safe, Dynamic Reduction in Aircraft Separation: NASA's Aircraft Vortex Spacing System (AVOSS)", National Aeronautics and Space Administration, 2001, NASA/TM-2001-211052.

Perry, RB, DA Hinton, RA Stuever, "NASA Wake Vortex Research for Aircraft Spacing," American Institute of Aeronautics and Astronautics, AIAA Paper 1997-0057.

Proctor, FH, "The Terminal Area Simulation System / Volume 1: Theoretical Formulation", National Aeronautics and Space Administration, 1987, NASA/CR-1987-4046.

Proctor, FH, "The NASA-Langley Wake Vortex Modelling Effort in Support of an Operational Aircraft Spacing System", American Institute of Aeronautics and Astronautics, AIAA Paper 1998-0589.

Proctor, FH, DW Hamilton, J Han, "Wake Vortex Transport and Decay in Ground Effect: Vortex Linking with the Ground," American Institute of Aeronautics and Astronautics, AIAA Paper 2000-0757.

Proctor, FH, DW Hamilton, GF Switzer, "TASS Driven Algorithms for Wake Prediction," American Institute of Aeronautics and Astronautics, AIAA Paper 2006-1073.

Proctor, FH, NN Ahmad, "Crosswind Shear Gradient Affect on Wake Vortices," American Institute of Aeronautics and Astronautics, AIAA Paper 2011-3038.

Pruis, MJ, DP Delisi, NN Ahmad, "Comparisons of Crosswind Velocity Profile Estimates Used in Fast-Time Wake Vortex Prediction Models," American Institute of Aeronautics and Astronautics, AIAA Paper 2011-1002. 2011a.

Pruis, MJ, DP Delisi, "Comparison of Ensemble Predictions of a New Probabilistic Fast-Time Wake Vortex Model and Lidar Observed Vortex Circulation Intensities and Trajectories," American Institute of Aeronautics and Astronautics, AIAA Paper 2011-3036. 2011b.

Pruis, MJ, DP Delisi, "Assessment of fast-time wake vortex prediction models using pulsed and continuous wave lidar observations at several different airports." American Institute of Aeronautics and Astronautics, AIAA Paper, 2011-3035. 2011c.

Pruis, MJ, DP Delisi, NN Ahmad, FH Proctor, "Atmospheric Turbulence Estimates from a Pulsed Lidar," American Institute of Aeronautics and Astronautics, AIAA Paper 2013-0512.

Pruis, MJ, DP Delisi "Observations of Small-scale Atmospheric Variability and the Importance of Accurate Weather Information in Deterministic and Probabilistic Fast-time Wake Vortex Modeling," American Institute of Aeronautics and Astronautics, AIAA Paper 2014-2468.

Robins, RE, DP Delisi, "NWRA AVOSS Wake Vortex Prediction Algorithm Version 3.1.1," National Aeronautics and Space Administration, 2002, NASA/CR 2002-211746.

Rossow, V, "Validation of Vortex-Lattice Method for loads on wings in lift-generated wakes", American Institute of Aeronautics and Astronautics, AIAA Paper 1994-1839.

Sarpkaya, T, "New Model for Vortex Decay in the Atmosphere," *Journal of Aircraft*, Vol. 37, 2000, pp. 53-61.

Sarpkaya, T, RE Robins, and DP Delisi, "Wake-Vortex Eddy-Dissipation Model Predictions Compared with Observations," *Journal of Aircraft*, Vol. 38, 2001, pp. 687- 692.

Schwarz, C, K Hahn, "Simplified Hazard Areas for Wake Vortex Encounter Avoidance", American Institute of Aeronautics and Astronautics, AIAA Paper 2005-5903.

Tatnall, CR, "A Proposed Methodology for Determining Wake-Vortex Imposed Aircraft Separation Constraints", MS Thesis, 1995, George Washington University.

van Baren, G, L Speijker, P van der Geest, "Wake vortex safety at NLR". NLR Air Transport Safety Institute. 2011.

van der Geest, P, "Wake vortex severity criteria: The search for a single metric", NLR Air Transport Safety Institute, February 2012.

Vicroy, DD, PM Vijgen, HM Reimer, JL Gallegos, PR Spalart, "Recent NASA Wake-Vortex Flight Tests, Flow Physics Database and Wake-Development Analysis," American Institute of Aeronautics and Astronautics, AIAA Paper 1998-5592.

von Mises, R, "Theory of Flight", Dover Publications, Inc., New York, 1959.

Wing, DJ, WB Cotton, "For Spacious Skies: Self-Separation with "Autonomous Flight Rules" in US Domestic Airspace", American Institute of Aeronautics and Astronautics, AIAA Paper 2011-6865.

Zak, JA, "Cases of Interesting Meteorological Conditions during Wake Vortex Measurements at Memphis, Tennessee during August 1995", Vigyan Interim Report for NASA Contract NAS1-19341. 1996.

REPORT DOCUMENTATION PAGE			Form Approved OMB No. 0704-0188		
<p>The public reporting burden for this collection of information is estimated to average 1 hour per response, including the time for reviewing instructions, searching existing data sources, gathering and maintaining the data needed, and completing and reviewing the collection of information. Send comments regarding this burden estimate or any other aspect of this collection of information, including suggestions for reducing this burden, to Department of Defense, Washington Headquarters Services, Directorate for Information Operations and Reports (0704-0188), 1215 Jefferson Davis Highway, Suite 1204, Arlington, VA 22202-4302. Respondents should be aware that notwithstanding any other provision of law, no person shall be subject to any penalty for failing to comply with a collection of information if it does not display a currently valid OMB control number.</p> <p>PLEASE DO NOT RETURN YOUR FORM TO THE ABOVE ADDRESS.</p>					
1. REPORT DATE (DD-MM-YYYY) 01-05-2016		2. REPORT TYPE Technical Memorandum		3. DATES COVERED (From - To)	
4. TITLE AND SUBTITLE A Coupled Probabilistic Wake Vortex and Aircraft Response Prediction Model			5a. CONTRACT NUMBER		
			5b. GRANT NUMBER		
			5c. PROGRAM ELEMENT NUMBER		
6. AUTHOR(S) Gloudemans, Thijs; Van Lochem, Sander; Ras, Eelco; Malissa, Joel; Ahmad, Nashat N.; Lewis, Timothy A.			5d. PROJECT NUMBER		
			5e. TASK NUMBER		
			5f. WORK UNIT NUMBER 330693.04.20.07.03		
7. PERFORMING ORGANIZATION NAME(S) AND ADDRESS(ES) NASA Langley Research Center Hampton, VA 23681-2199			8. PERFORMING ORGANIZATION REPORT NUMBER L-20687		
9. SPONSORING/MONITORING AGENCY NAME(S) AND ADDRESS(ES) National Aeronautics and Space Administration Washington, DC 20546-0001			10. SPONSOR/MONITOR'S ACRONYM(S) NASA		
			11. SPONSOR/MONITOR'S REPORT NUMBER(S) NASA-TM-2016-219193		
12. DISTRIBUTION/AVAILABILITY STATEMENT Unclassified - Unlimited Subject Category 03 Availability: NASA STI Program (757) 864-9658					
13. SUPPLEMENTARY NOTES					
14. ABSTRACT Wake vortex spacing standards along with weather and runway occupancy time, restrict terminal area throughput and impose major constraints on the overall capacity and efficiency of the National Airspace System. The National Aeronautics and Space Administration has been conducting research on characterizing wake vortex behavior in order to develop wake decay and transport prediction models. This paper presents a methodology for the development and integration of probabilistic wake vortex model with an aircraft response model for air traffic management applications. The two modules of the proposed system 1) probabilistic wake prediction, and 2) aircraft response to wake vortex encounter, are evaluated independently using data from field experiments and wind tunnel tests with favorable results. The methodology as described in this report is well-suited for systems-level design and safety analysis of new advanced air traffic management concepts as well as forensic reconstruction of accidents due to inadvertent wake encounters. It is also envisioned that at a later stage of maturity, these models could potentially be used operationally, in ground-based spacing and scheduling systems as well as on the flight deck.					
15. SUBJECT TERMS Probabilistic wake model; Wake encounter model; Wake turbulence					
16. SECURITY CLASSIFICATION OF:			17. LIMITATION OF ABSTRACT	18. NUMBER OF PAGES	19a. NAME OF RESPONSIBLE PERSON
a. REPORT	b. ABSTRACT	c. THIS PAGE			STI Help Desk (email: help@sti.nasa.gov)
U	U	U	UU	56	19b. TELEPHONE NUMBER (Include area code) (757) 864-9658